# Article

# Metabolic trait diversity shapes marine biogeography

Curtis Deutsch[1,2 ✉], Justin L. Penn[1] & Brad Seibel[3]

Climate and physiology shape biogeography, yet the range limits of species can rarely be ascribed to the quantitative traits of organisms[1–3]. Here we evaluate whether the geographical range boundaries of species coincide with ecophysiological limits to acquisition of aerobic energy[4] for a global cross-section of the biodiversity of marine animals. We observe a tight correlation between the metabolic rate and the efficacy of oxygen supply, and between the temperature sensitivities of these traits, which suggests that marine animals are under strong selection for the tolerance of low $O_2$ (hypoxia)[5]. The breadth of the resulting physiological tolerances of marine animals predicts a variety of geographical niches—from the tropics to high latitudes and from shallow to deep water—which better align with species distributions than do models based on either temperature or oxygen alone. For all studied species, thermal and hypoxic limits are substantially reduced by the energetic demands of ecological activity, a trait that varies similarly among marine and terrestrial taxa. Active temperature-dependent hypoxia thus links the biogeography of diverse marine species to fundamental energetic requirements that are shared across the animal kingdom.

The provisioning of energy to organisms in their natural environment is a key determinant of fitness. The energetic demands of ectothermic organisms increase with temperature and activity, and must be met by an adequate supply of oxygen ($O_2$) and food. At a minimum, physiological survival requires that the supply of energy matches the maintenance costs of an organism in a resting state; these energy demands vary by body size, temperature and species[6,7]. Additional energetic costs are incurred by the growth and activity required for ecological survival, which depend on lifestyle and ecological niche and typically increase energy expenditure several-fold above resting rates[8,9].

Energy provision can be limited by $O_2$ if its availability falls short of the metabolic demands of the organism, inducing a hypoxic condition[10–12]. This is more common in aquatic environments due to the slower diffusion of $O_2$ in water than in air[13]. The effects of an acute reduction in $O_2$ on population fitness can induce considerable die-offs[14,15]; however, the presence of metabolic barriers in habitats under stable conditions are difficult to observe. Recent analyses suggest that the current latitude and depth limits of several marine ectothermic species coincide with an $O_2$ pressure that is just adequate to fuel the energy demand for physiological maintenance and sustained ecological activity[4,16,17]. Here we evaluate the metabolic causes and biogeographical consequences of the constraints to aerobic energy by combining a mathematical model of temperature-dependent hypoxia with laboratory and field data from the broadest-available diversity of marine animal species.

## Temperature-dependent $O_2$ tolerance

The aerobic energy balance of an organism can be represented by a Metabolic Index[4] ($\Phi$), which is defined as the ratio of $O_2$ supply to resting demand (Fig. 1a and Methods):

$$\Phi = \frac{\alpha_S}{\alpha_D} B^\varepsilon p_{O_2} \exp\left\{ \frac{E_o}{k_B}\left[ \frac{1}{T} - \frac{1}{T_{ref}} \right] \right\} \qquad (1)$$

where $\alpha_D$ is the resting metabolic rate per unit body mass ($B$) at a reference temperature ($T_{ref}$), and $\alpha_S$ is the efficacy of $O_2$ supply per unit body mass and the $O_2$ pressure ($p_{O_2}$) of the ambient medium (units are described in Fig. 1 and the Methods). The ratio of $\alpha_D/\alpha_S$ defines a first key physiological trait of an organism: its resting vulnerability to hypoxia at the reference temperature, $V_h = \alpha_D/\alpha_S$, which is measurable as the lowest $O_2$ pressure ($P_{crit}$) that can sustain resting metabolic demand ($\Phi = 1$) (Fig. 1a). The inverse of hypoxia vulnerability is hypoxia tolerance, which is denoted $A_o = 1/V_h$, as defined previously[4]. A second key trait, $E_o$, is the sensitivity of hypoxia vulnerability to temperature ($T$), which is described by the exponential Arrhenius function (Fig. 1a) (Boltzmann constant, $k_B$) and is equal to the difference between the temperature variation in the metaboli4c rate ($E_d$) and the $O_2$ supply ($E_s$), such that $E_o = E_d - E_s$ (Methods). The exponent $\varepsilon$ is the allometric scaling of the supply-to-demand ratio, which is typically near zero[18].

A third component of the energetic balance of an organism is the $O_2$ needed to fuel growth and essential ecological activities. In terrestrial animals, sustained metabolic rates range from 1.5 to 7 times those at rest, a ratio termed the sustained metabolic scope (SMS)[8,9]. For aquatic aerobic organisms, such levels of activity would increase the resting vulnerability to hypoxia from $V_h$ to a higher value, $V_h \times$ SMS, which requires that the minimum $\Phi$ of a given species in its environment increases above its resting minimum (which is set to 1, see above) by the same factor, denoted $\Phi_{crit}$. The ratio SMS will depend on the ecology and life history of each species. This ecological trait is not directly
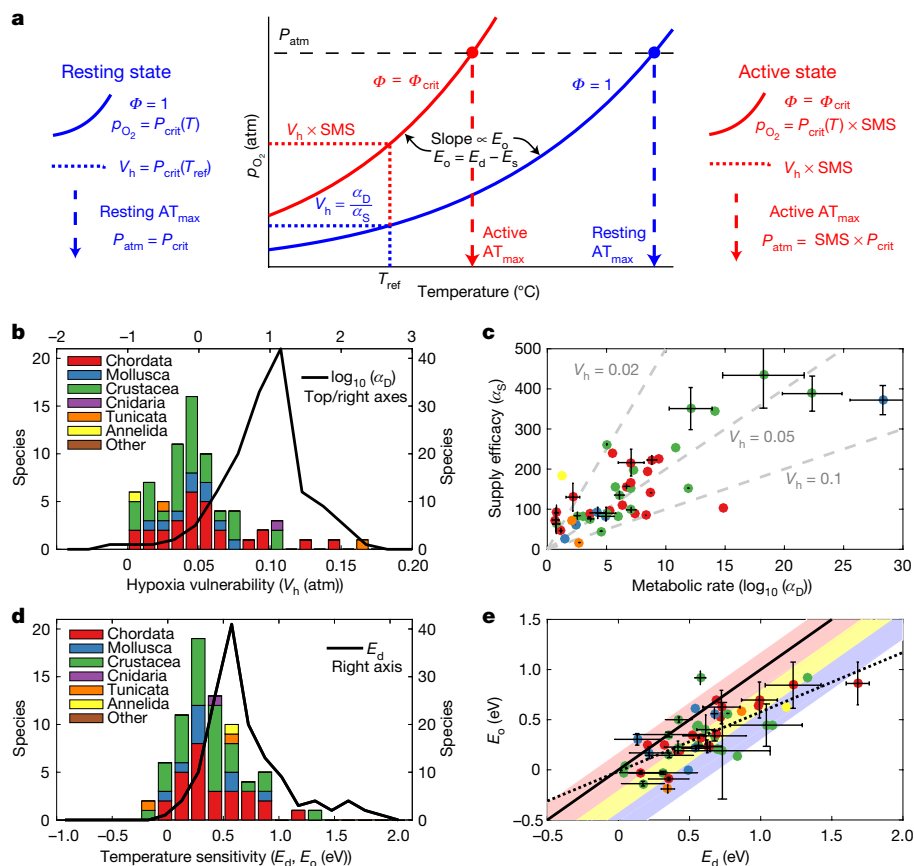
**Fig. 1 | Relationships among species traits that govern the temperature-dependent vulnerability to hypoxia of marine animals. a**, Curves of constant Metabolic Index ($\Phi$) trace the $p_{O_2}$ required to satisfy the $O_2$ demand of species for resting (blue) or active (red) metabolic rates. **b–e**, The resting curve of each species is defined by a hypoxia vulnerability ($V_h$) and its temperature sensitivity ($E_o$), each of which reflect separate traits for $O_2$ supply and demand (**b**, **d**) and their covariation (**c**, **e**). Active curves, which are increased from the resting curve by sustained activity (SMS), require a correspondingly higher $\Phi$ ($\Phi_{crit}$) (Fig. 4). The intersection of $\Phi$ curves with atmospheric $p_{O_2}$ define the upper thermal limits of aerobic metabolism (AT$_{max}$) (Fig. 5). **b**, **c**, Hypoxia vulnerability ($V_h$; atm) and $O_2$ demand at rest (**b**; $\alpha_D$; μmol $O_2$ h$^{-1}$ g$^{-3/4}$, log$_{10}$ scale) vary widely among species but are uncorrelated because the metabolic rate and the efficacy of the $O_2$ supply (**c**; $\alpha_S$; μmol $O_2$ h$^{-1}$ g$^{-3/4}$ atm$^{-1}$) are strongly correlated (Extended Data Table 1). **d**, The temperature dependence of the hypoxia vulnerability ($E_o$; eV)

is shifted to lower values than that of resting metabolic rate ($E_d$; eV) because the $O_2$ supply accelerates with temperature (that is, $E_s = E_d - E_o > 0$), partially compensating the thermal rise in metabolic demand. **e**, The relationship between $E_o$ and $E_d$ (dotted line; slope < 1) (Extended Data Table 1) suggests that species with a stronger metabolic response to temperature also exhibit stronger compensatory $O_2$ supply mechanisms (Extended Data Fig. 2b). Values of $E_s$ are within the range predicted for diffusion (yellow shading) and empirically estimated from rates of the ventilation and circulation of animals in cool waters (blue shading; 0.55 ± 0.15 eV (mean ± s.d.)) and warm waters (red shading; 0.04 ± 0.18 eV (mean ± s.d.)) (Extended Data Fig. 3). **c**, **e**, Data (points and error bars, or centred dot, if the error bars are shorter than marker) are mean ± s.e.m. for species with $n > 2$ temperature values. See Supplementary Table 1 for the number of independent experiments for each species, and Extended Data Table 1 for statistics on the two-sided $t$-tests of the trait correlations.

measured in marine species, but it can be estimated from the maximum metabolic rates, while $\Phi_{crit}$ can be inferred as the lowest value of $\Phi$ that bounds the geographical distribution of a species[4]. If values of $\Phi_{crit}$ match those of SMS, this strongly indicates that there is an energetic limit on marine species habitats.

To characterize the variation in these traits across diverse marine animal species, we analysed published physiological rates and thresholds (Methods), and the global geographical distributions of the species (OBIS; https://obis.org/). The dataset of 199 species includes 145 species with temperature-dependent metabolic rates and associated parameters ($E_d$ and $\alpha_D$; hereafter called 'metabolic traits') (Extended Data Fig. 1a) and 72 species with temperature-dependent hypoxia thresholds and corresponding parameters ($E_o$ and $V_h$; hereafter called 'hypoxic traits') (Extended Data Fig. 1b and Supplementary Table 1). The species span more than eight orders of magnitude in body size, inhabit all ocean basins and biomes (Extended Data Fig. 1c), belong to five phyla (Annelida, Arthropoda, Chordata, Cnidaria and Mollusca) and broadly but incompletely sample the metabolic, geographical and taxonomic diversity of the ocean.

## Physiological trait diversity

Resting metabolic rates normalized by temperature and body mass vary by orders of magnitude among all 145 species (Fig. 1b), but remain within the range found across the tree of life[19]. The critical $O_2$ pressures also show a well-defined distribution of resting hypoxia vulnerability across species (Fig. 1b). Although metabolic rates are a direct driver of hypoxia vulnerability, the two traits are uncorrelated across species, and $\alpha_D$ exhibits greater interspecies variation than does $V_h$. These observations suggest that animals with a high metabolism also have a high efficacy of $O_2$ delivery. Indeed, the absolute metabolic rates and coefficients of $O_2$ supply are highly correlated among species (Fig. 1c and Extended Data Table 1), which indicates that there is a strong selective pressure for tolerance to low $O_2$, even for species that live outside relatively small ocean regions commonly termed hypoxic zones[20].

The temperature sensitivity of metabolic rates within species exhibits substantial variation across species (Fig. 1d). The mean value, standard deviation and range of $E_d$ (0.69 ± 0.36 eV, 0.1–2.0 eV) are similar to the thermal acceleration of the metabolic rates of organisms that are
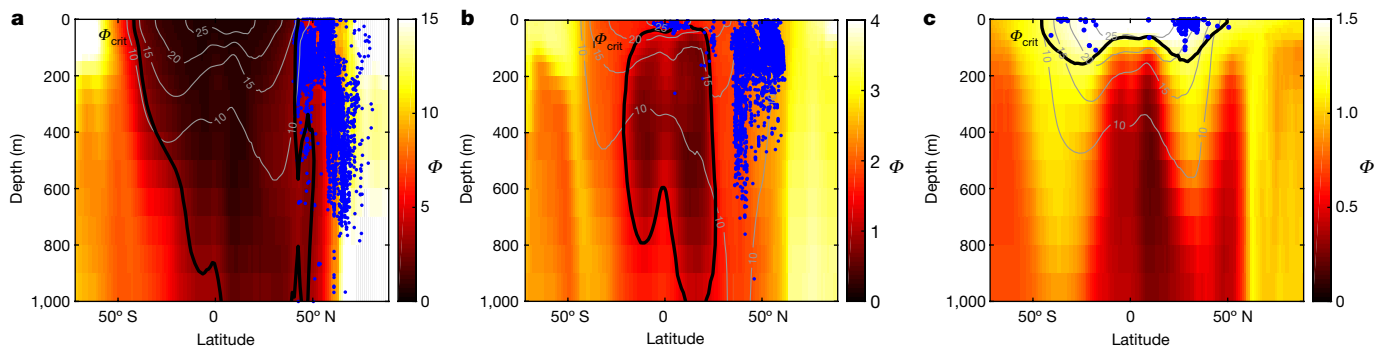
**Fig. 2 | Spatial distributions of the Metabolic Index and species with distinct temperature sensitivities. a**, Northern shrimp (*Pandalus borealis*) from the north Atlantic, Pacific and Arctic Oceans. **b**, Small-spotted catshark (*Scyliorhinus canicula*) from the eastern Atlantic Ocean and Mediterranean Sea. **c**, Sea squirt (*S. plicata*), a cosmopolitan tunicate. The Metabolic Index is computed from monthly climatological measurements using the traits of each species, and averaged annually and over its longitudinal range in OBIS (http://iobis.org) for mapping (northern shrimp, 180°–45° E; catshark,

20° W–15° E; sea squirt, all longitudes). The species have similar hypoxia vulnerability ($V_h$, around 0.10–0.16 atm), but their temperature sensitivities ($E_o$) vary widely (northern shrimp, $E_o \approx 0.9$; catshark, $E_o \approx 0.2$; sea squirt, $E_o \approx -0.2$) yielding different $\Phi$ gradients across latitude and depth. A single lower limit of $\Phi$ bounding each species range is contoured ($\Phi_{crit}$; black lines), along with climatological isotherms (grey lines, in °C) and observed species occurrences (blue dots) (Methods).

observed across the tree of life[21]. The temperature sensitivity of hypoxia vulnerability also varies widely across species (Fig. 1d), but $E_o$ has a smaller mean, standard deviation and range ($0.4 \pm 0.28$, $-0.2$–$1.3$ eV) that includes negative values. The differences in $E_o$ relative to $E_d$ reflect the effect of temperature on $O_2$ supply ($E_s$), the positive mean value ($0.29 \pm 0.23$ eV) of which suggests that the supply of $O_2$ also accelerates with temperature[22]. The temperature effect on the supply of $O_2$ therefore counteracts, and for species with $E_o < 0$, even exceeds the thermal increase in metabolic rates.

To confirm the role of the $O_2$ supply in moderating the temperature sensitivity of the vulnerability to hypoxia, we estimated the thermal response of three processes that transport $O_2$ from ambient fluid to body tissue: the ventilation of water past the organism, the diffusion of $O_2$ through the boundary layer at the water–body interface and the internal transport of $O_2$ by animals that have circulatory systems. Diffusive $O_2$ fluxes increase with temperature in proportion to gas diffusivity ($\kappa$) and increase inversely to the decrease in kinematic viscosity ($v$). The ratio of gas diffusivity to kinematic viscosity—the Schmidt number (Sc = $v/\kappa$)—predicts a diffusive $O_2$ flux[23] for which the temperature dependence, $E_s$, lies between 0.21 and 0.42 eV (Extended Data Fig. 3a). This range encompasses the mean value of $E_s$ that was inferred from all species for which $E_o$ and $E_d$ can both be estimated (Fig. 1e), but cannot account for its full interspecies range.

The ventilation of $O_2$ to and circulation in the body may also modify the temperature sensitivity of hypoxia tolerance[24–27] (Extended Data Fig. 3b). Both ventilation and circulation rates increase with temperature in cooler waters ($E_s = 0.55 \pm 0.15$ eV (mean ± s.d.)) (Fig. 1e and Extended Data Fig. 3c), but the response decreases or even reverses in warmer conditions ($E_s = 0.04 \pm 0.18$ eV (mean ± s.d.)) (Fig. 1e and Extended Data Fig. 3c). These thermal responses of the $O_2$ supply combined with those of metabolic demand ($E_d$) can account for nearly the entire range of the temperature-dependence of hypoxia vulnerability ($E_o$). Moreover, the stronger thermal response of the ventilation and circulation rates in cool compared with warm waters is consistent with the weaker temperature sensitivity of species vulnerability to hypoxia (lower $E_o$) that is observed under cold relative to warm conditions (Extended Data Fig. 3d). Thus, both biological and physical responses of the $O_2$ supply to temperature reduce the temperature sensitivity of hypoxia vulnerability, relative to that of the metabolic demand alone. The compensation of faster metabolic rates at higher temperatures by a more rapid $O_2$ supply indicates that there is a strong selective pressure for oxygen supply to meet demand across the range of inhabited temperatures.

## Linking physiology to biogeography

The variation in temperature-dependent hypoxia traits suggests that species experience distinct geographical patterns of hypoxia risk (Fig. 2). In the upper ocean, both temperature and $p_{O_2}$ decrease with depth, but often have opposing gradients with latitude; temperature decreases as subsurface $p_{O_2}$ increases away from the Equator. The resulting spatial variation in $\Phi$ depends on the strength of these gradients, and on the temperature sensitivity parameter, $E_o$. For species with strongly positive values of $E_o$, $\Phi$ decreases towards the warm low-$O_2$ waters of the shallow tropics (Fig. 2a). However, positive $E_o$ also weakens any vertical decrease in $\Phi$, because the decline in ambient $O_2$ is compensated by a slower metabolic rate, which extends the potential habitat of species into deeper waters. By contrast, for species with $E_o < 0$, the highest $\Phi$ is found in tropical waters, but declines rapidly with depth below the surface due to both lower $O_2$ levels and cooler temperatures (Fig. 2c). The diversity in temperature-dependent hypoxia traits suggests that species that are limited by low $\Phi$ conditions may occupy distinct ocean habitats with global coverage, from shallow tropical waters to high-latitude and deep water, with a continuum of patterns in between (Fig. 2b).

To test whether the range of the predicted geographical habitat niches corresponds to the actual distributions of marine species, we extracted global occurrence data[14] for all species in the physiological database. For the 72 species with Metabolic Index parameters ($E_o$, $V_h$), distribution data were available for most species ($n = 68$), and the sampling resolution of many species was sufficient to reveal clear range boundaries in depth and latitude (Fig. 2 and Extended Data Figs. 4, 5). These data include three species that have similar $V_h$ but span the full range of $E_o$, from strongly positive ($E_o = 0.9$, northern shrimp) to slightly negative ($E_o = -0.2$, sea squirt) and an intermediate value ($E_o = 0.2$, small-spotted catshark), which predict the distinct aerobic habitat distributions of these species (Fig. 2). In all three species, range boundaries in latitude and in depth are closely aligned with a single value of $\Phi$ above which the populations are widely distributed and below which reported occurrences are rare and isolated. Geographical range boundaries across a range of depths, latitudes and longitudes also coincided with single isopleths of $\Phi$ in other well-mapped species (Extended Data Fig. 4), including species that span multiple ocean basins or different sides of the same basin (Extended Data Fig. 5).

The boundaries of the geographical ranges of species are more strongly aligned with the Metabolic Index than with either temperature or $p_{O_2}$ alone (Fig. 2 and Extended Data Figs. 4–7). This can be observed geographically: in vertical cross-sections, range boundaries follow a
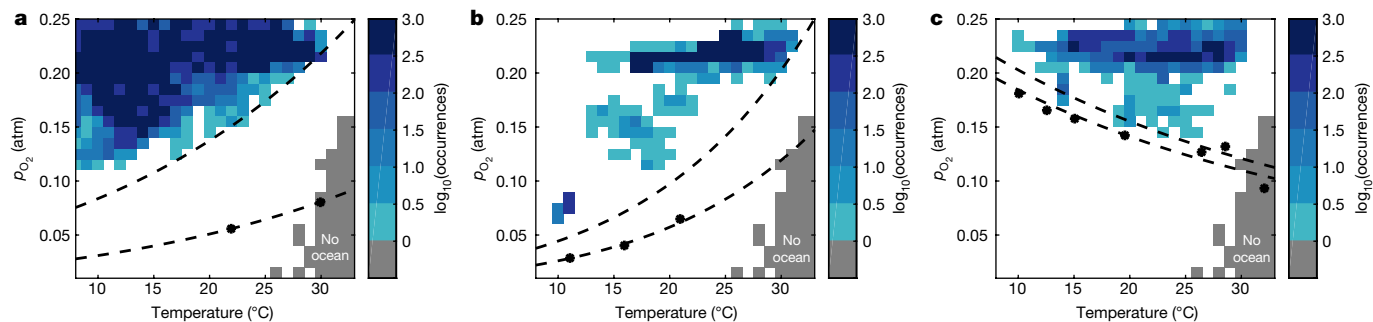
**Fig. 3 | Temperature and $p_{O_2}$ state-space habitat for three marine species from different phyla, ocean basins and latitude ranges. a**, Summer flounder (*Paralichthys dentatus*), a fish from the subtropical eastern Atlantic Ocean. **b**, Nautilus (*Nautilus pompilius*), a mollusc from the tropical Indo-Pacific Ocean. **c**, Sea squirt (*S. plicata*), a cosmopolitan tunicate. The frequency of reported occurrences of each species ($\log_{10}$-transformed values) at each temperature (°C) and $p_{O_2}$ level (atm) is coloured. Water conditions with no reported occurrences of the species are white, and localities with no modern ocean volume are shaded grey. Measured critical $p_{O_2}$ levels ($P_{crit}$; black dots)

indicate the measured threshold for maintaining the resting metabolic rate in laboratory experiments (Supplementary Table 1) and are fitted to the Metabolic Index (equation (1)) when $\Phi = 1$ (bottom dashed lines). The boundaries of inhabited ocean conditions follow a Metabolic Index curve, which is elevated above the $P_{crit}$ curve by a factor $\Phi_{crit}$ (top dashed lines) that represents the ratio of the active-to-resting metabolic rate. Contrary to observations, a species for which the range is limited by temperature or $p_{O_2}$ alone would have a state-space occupancy delineated by a vertical or horizontal line, respectively.

constant $\Phi$ value, but tend to cross multiple isotherms (Fig. 2 and Extended Data Figs. 4, 6). In mid-latitude species, range boundaries lean equatorward at shallower depths, opposite to the poleward tilt of isotherms (Fig. 2a, b and Extended Data Fig. 4a–e). At the surface, range limits can be reached as $\Phi$ declines towards the Equator, even without a gradient in $p_{O_2}$ (Extended Data Figs. 4a–e, 6a, c).

The alignment of range boundaries with $\Phi$ is most easily observed, however, by projecting the biogeography of species onto the temperature and $p_{O_2}$ state–space that they inhabit (Fig. 3). Across species from distinct phyla and multiple ocean basins, including those with sparse spatial sampling, the state-space habitat map reveals strong correlations between the temperatures and $p_{O_2}$ levels that bound the occurrences of species. These relationships are consistent with the expectations based on the Metabolic Index of each species, with opposite slopes for species with positive and negative $E_o$ values, but are incongruent with habitat limitation by either a single temperature or $p_{O_2}$ level. The predictive ability of $\Phi$ to discriminate between inhabited and uninhabited ocean regions is better than that of temperature for 92% of species, better than $p_{O_2}$ for 67% of species, and better than both temperature and $p_{O_2}$ for 62% of species (Methods and Extended Data Fig. 7).

That the species habitat boundaries coincide with a lower $\Phi$ value suggests that an aerobic barrier limits the geographical ranges of marine animals (Figs. 2, 3). We determined the range-bounding value, $\Phi_{crit}$, for all of the species with hypoxia traits and georeferenced location data, using two independent methods that yield convergent results (Methods and Extended Data Fig. 8a, b). The average of $\Phi_{crit}$ is approximately 3.3 (interdecile range, 1.3–6.5) (Fig. 4). For all species, waters with lower $\Phi$ values exist within their inhabited depth range, but lack confirmed sightings (Extended Data Fig. 8c).

If $\Phi_{crit}$ is the operative habitat barrier for marine species, its values should correspond to their sustained metabolic rates relative to rest. Long-term energetic demand is not directly measured for marine organisms, but short-term experimental estimates of maximum-to-resting rate ratios (MMR/RMR) provide an empirical upper bound on SMS (Methods). We find a strong correlation between biogeographically inferred $\Phi_{crit}$ and laboratory measured MMR/RMR values (Extended Data Fig. 9 and Extended Data Table 1), which suggests that SMS lies approximately midway between the resting and maximum rates (that is, SMS $= w_R + (1 - w_R)(MMR/RMR)$; (see Methods, equation 7); $w_R = 0.4 \pm 0.17$ (mean ± s.d.), $n = 14$) (Extended Data Fig. 9), consistent with independent estimates of SMS from carbon isotopes in the otoliths of Atlantic cod[28]. Applied to the broadest compilation of MMR/RMR

ratios, this scaling yields an interspecies distribution of SMS ($n = 106$) (Fig. 4a) that is statistically indistinguishable from that of $\Phi_{crit}$ (Fig. 4a, Extended Data Table 1). The $\Phi_{crit}$ values of the few sessile species that we analysed (*Styela plicata*, *Lophelia pertusa* and *Crassostrea gigas*) were among the lowest (Fig. 3c and Supplementary Table 1), which is consistent with their less-active lifestyles. Together, these observations provide strong evidence that $\Phi_{crit}$ corresponds to SMS, and thus represents an energetic barrier to the geographical ranges of species.

The interpretation of $\Phi_{crit}$ as the ratio of sustained active-to-resting metabolic rates can be further evaluated by comparing its frequency distribution across marine species to the SMS data that were directly and independently measured for terrestrial taxa[4,8], including mammals, birds and reptiles (Fig. 4b). The available data reveal no significant differences between the distribution of marine $\Phi_{crit}$ and marine and terrestrial SMS distributions (Fig. 4, Extended Data Table 1), which supports the suggestion that $\Phi_{crit}$ is an operative limit on the geographical ranges of marine species. These results also suggest that the ratios of active-to-resting metabolic rates are a fundamental trait that represents ecological and life-history variation across the animal kingdom.

The SMS of marine taxa has important implications for empirical metrics of thermal tolerance that are widely used to infer the climate sensitivity of marine species. By elevating $O_2$ demand, ecological and life-history activity increases the vulnerability to hypoxia from a resting threshold ($V_h$), to an active one, $V_h \times \Phi_{crit}$, that is a key operative constraint on marine geographical ranges. Similarly, because hypoxia tolerance decreases with temperature for most species, ecological activity also reduces the maximum temperature at which aerobic metabolism can be sustained. Maximum temperatures for aerobic metabolism can be derived from the Metabolic Index (Fig. 1a) as the temperature at which $P_{crit}$ reaches the atmospheric $O_2$ pressure ($P_{atm}$) applied in experimental determinations of thermal tolerance[29] (Methods). The distribution of this aerobic thermal limit, denoted $AT_{max}$, evaluated in a resting state ($\Phi = 1$, $AT_{max}^{rest}$) is highly variable among species (Fig. 5a), owing to the diversity of hypoxia traits ($E_o$ and $V_h$). For all species, $AT_{max}^{rest}$ is considerably higher than the temperatures that are encountered by the organisms in their natural habitats[30,31], and for most species it is higher than temperatures found in the ocean (Fig. 5a). Similar findings have been reported based on observed critical thermal maxima, termed $CT_{max}$, measured by the loss of physiological performance in a resting state[32]. Indeed, the frequency distributions of $AT_{max}^{rest}$ and $CT_{max}$ are remarkably similar (Fig. 5a and Extended Data Fig. 4a–d). In four of the seven species for which both thermal tolerance metrics
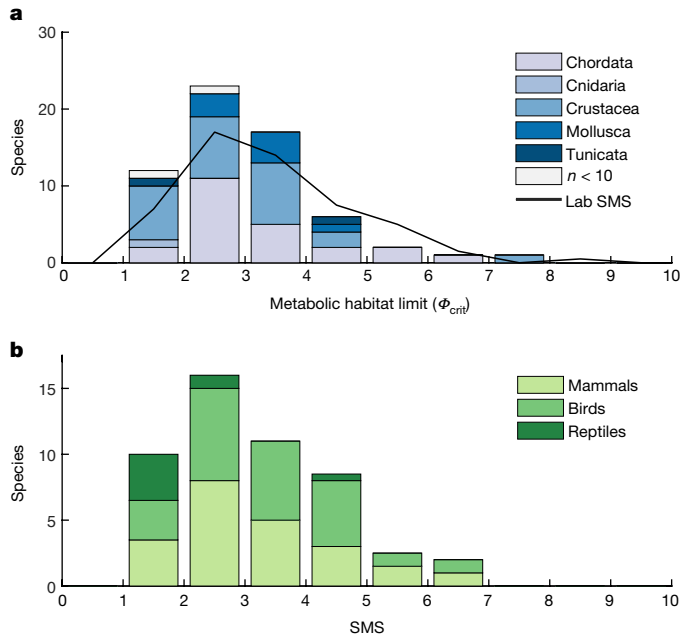
**Fig. 4 | Diversity of the ecological trait governing energetic habitat barriers.** **a**, Histograms of the lowest values of $\Phi$ in the habitat of a species—that is, $\Phi_{crit}$ (bars, light grey for species with fewer than 10 occurrences)—and SMS estimated from measurements of maximum-to-resting metabolic rate ratios[41] (line; see Methods). **b**, Histogram of SMS for terrestrial species determined in field studies[8,9]. The interspecies distributions of $\Phi_{crit}$ are indistinguishable from those of marine and terrestrial SMS (Extended Data Table 1), suggesting that $\Phi$ is the operative limit that most frequently acts on the warm temperature and low $O_2$ edge of the geographical range of marine species (but see Fig. 3c).

are known, $AT_{max}^{rest}$ occurs at a temperature at or below $CT_{max}$ (Extended Data Fig. 10). This correspondence may reflect an aerobic basis for thermal tolerance[29], although the link remains controversial[25–36]. Whatever the underlying physiological basis for this similarity, both measures suggest that although there is a large 'thermal safety margin' in the face of climate warming[37,38], these are derived from, and applicable to, only a state of rest.

Under the ecologically relevant energetic demand ($\Phi = \Phi_{crit}$), the active aerobic thermal maximum, $AT_{max}^{act}$, falls well below $AT_{max}^{rest}$ (Fig. 5b). Indeed, calculated values of $AT_{max}^{act}$ closely correspond to the maximum occupied environmental temperatures of individual species (Extended Data Fig. 10). Across species, the distribution of $AT_{max}^{act}$ tracks the global volumetric frequency of ocean temperatures. Thus, species with substantial apparent thermal safety margins at rest are in fact likely to be at the limit of their active thermal tolerance in the ocean[39] and will experience habitat compression even at modest levels of warming and without any depletion of $O_2$.

## Implications

The energetic balance of organisms is a powerful framework for explaining biogeographical patterns from temperature-dependent hypoxic tolerances and constituent metabolic rates that have been well studied for decades[4–6]. Geographical range limits imposed by aerobic energy constraints apply to a greater diversity of ocean species, physiologies and habitats than previously investigated[4,16], from tropical to high-latitude waters and from shallow to deep ocean niches. Our results thus extend and strengthen the hypothesis that temperature-dependent hypoxia has a major role in biogeography, by mediating how ocean temperature and $O_2$ are experienced by organisms with diverse environmental tolerances and geographical niches. The global applicability of such
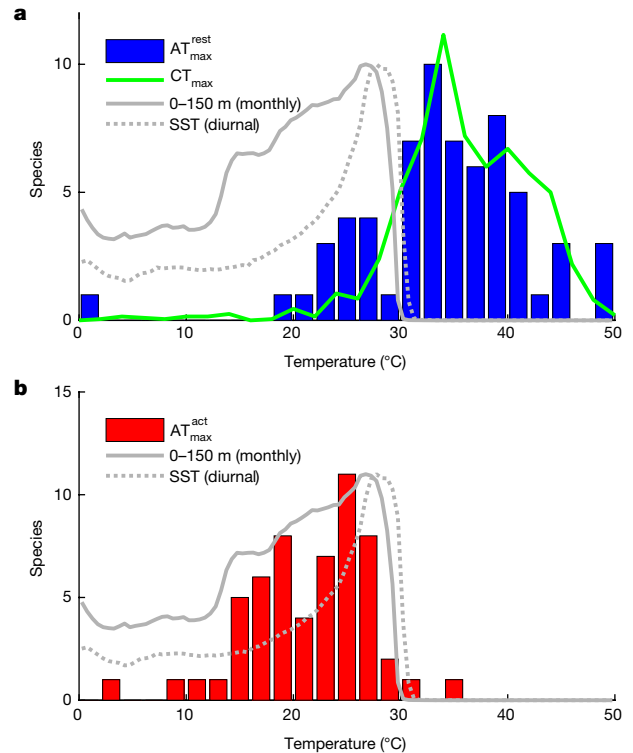
**Fig. 5 | Thermal tolerance of species measured in laboratory studies ($CT_{max}$) and predicted from the Metabolic Index ($AT_{max}$). a**, Histograms of the aerobic thermal maxima at rest ($AT_{max}^{rest}$; coloured bars) of species derived from measured hypoxia traits and critical thermal maxima ($CT_{max}$; green line), which were derived from loss of physiological function experiments. Grey lines depict the relative frequency of global upper ocean temperatures (solid, monthly depth-resolved upper 150 m; dotted, satellite-based daytime Sea Surface Temperature (Methods), scaled to the peak number of species for visualization. **b**, Active $AT_{max}$ based on the hypoxia traits and $\Phi_{crit}$ of all species. Activity levels reduce thermal tolerance from values well above ocean temperatures (grey lines) for species at rest (**a**) to temperatures that limit species ranges (**b**). $AT_{max}$ is the maximum aerobic temperature permitting atmospheric $p_{O_2}$ to meet resting or active metabolic $O_2$ demands, computed (see Methods) by solving for $T$ in equation (1), with $p_{O_2} = P_{atm}$ and $\Phi = 1$ (for resting $AT_{max}^{rest}$) or $\Phi = \Phi_{crit}$ (for active $AT_{max}$).

constraints support their use to predict patterns of extinction caused by climate change in the geological record[40] and in the future.

Sustained activity levels and the metabolic traits—the resting metabolic rate and its temperature sensitivity—that underlie aerobic energy barriers are not substantially different from the values observed in terrestrial biota. However, the hypoxia traits that shape those energetic barriers—resting hypoxia vulnerability and its temperature sensitivity—cannot be derived from metabolic traits alone because of the strong compensation by $O_2$ supply mechanisms. Species with fast metabolisms exhibit rapid $O_2$ supply rates (Fig. 1c and Extended Data Fig. 2), while those with high metabolic temperature sensitivities show strong thermal responses of $O_2$ extraction (Fig. 1e and Extended Data Fig. 2). The constituent traits of active hypoxia vulnerability are also correlated: species with a lower resting hypoxia vulnerability have a higher active to resting metabolic rate ratio (Extended Data Fig. 2). These correlations act to narrow the interspecies ranges of all three key traits (Extended Data Fig. 2) and suggest that there are strong physiological trade-offs and selective pressures, the nature and causality of which remain unresolved. Whatever their mechanistic origins, these trade-offs and constraints have resulted in a breadth of temperature-dependent hypoxia tolerance and associated spatial habitat limits that allow species to collectively exploit the full range of aerobic conditions found in the modern ocean.

# Article

The data needed to calibrate the Metabolic Index and diagnose the relative role of $O_2$ supply and demand can be derived from standard respirometry data, but currently the number of sampled species comprises only a small fraction of the total marine biodiversity. They include few species without circulatory systems; species without a clear $P_{crit}$ ('oxyconformers'); or species pairs with well-characterized predator–prey or other ecological relationships that may modulate the physiological response to climate change. A systematic and concerted effort to expand data on Metabolic Index parameters across a wider variety of marine biota, especially those with rich biogeographical data, and populations that may adapt hypoxia traits over regional scales or between generations, will be key to further evaluating the role of temperature-dependent hypoxia in shaping marine biogeography, ecological interactions and habitat loss in a warming climate.

## Online content

1. Violle, C., Reich, P. B., Pacala, S. W., Enquist, B. J. & Kattge, J. The emergence and promise of functional biogeography. *Proc. Natl Acad. Sci. USA* **111**, 13690–13696 (2014).
2. Angilletta, M. J. *Thermal Adaptation: A Theoretical and Empirical Synthesis* (Oxford Univ. Press, 2009).
3. Sunday, J. M., Bates, A. E. & Dulvy, N. K. Global analysis of thermal tolerance and latitude in ectotherms. *Proc. R. Soc. B* **278**, 1823–1830 (2011).
4. Deutsch, C., Ferrel, A., Seibel, B., Pörtner, H.-O. & Huey, R. B. Ecophysiology. Climate change tightens a metabolic constraint on marine habitats. *Science* **348**, 1132–1135 (2015).
5. Mandic, M., Todgham, A. E. & Richards, J. G. Mechanisms and evolution of hypoxia tolerance in fish. *Proc. R. Soc. B* **276**, 735–744 (2009).
6. Seibel, B. A. & Drazen, J. C. The rate of metabolism in marine animals: environmental constraints, ecological demands and energetic opportunities. *Phil. Trans. R. Soc. Lond. B* **362**, 2061–2078 (2007).
7. Brey, T. An empirical model for estimating aquatic invertebrate respiration. *Methods Ecol. Evol.* **1**, 92–101 (2010).
8. Peterson, C. C., Nagy, K. A. & Diamond, J. Sustained metabolic scope. *Proc. Natl Acad. Sci. USA* **87**, 2324–2328 (1990).
9. Hammond, K. A. & Diamond, J. Maximal sustained energy budgets in humans and animals. *Nature* **386**, 457–462 (1997).
10. Fry, F. E. J. Effect of the environment on animal activity. *Univ. Tor. Stud. Biol. Ser.* **55**, 1–62 (1947).
11. Brett, J. R. Energetic responses of salmon to temperature. A study of some thermal relations in the physiology and freshwater ecology of sockeye salmon (*Oncorhynchus nerka*). *Am. Zool.* **11**, 99–113 (1971).
12. Pörtner, H.-O. & Farrell, A. P. Physiology and climate change. *Science* **322**, 690–692 (2008).
13. Piiper, J., Dejours, P., Haab, P. & Rahn, H. Concepts and basic quantities in gas exchange physiology. *Respir. Physiol.* **13**, 292–304 (1971).
14. Chan, F. et al. Emergence of anoxia in the California current large marine ecosystem. *Science* **319**, 920 (2008).
15. Diaz, R. J. & Rosenberg, R. Spreading dead zones and consequences for marine ecosystems. *Science* **321**, 926–929 (2008).
16. Wishner, K. F. et al. Ocean deoxygenation and zooplankton: very small oxygen differences matter. *Sci. Adv.* **4**, eaau5180 (2018).
17. Howard, E. M. et al. Climate-driven aerobic habitat loss in the California current system. *Sci. Adv.* **6**, eaay3188 (2020).
18. Nilsson, G. E. & Östlund-Nilsson, S. Does size matter for hypoxia tolerance in fish? *Biol. Rev. Camb. Philos. Soc.* **83**, 173–189 (2008).
19. DeLong, J. P., Okie, J. G., Moses, M. E., Sibly, R. M. & Brown, J. H. Shifts in metabolic scaling, production, and efficiency across major evolutionary transitions of life. *Proc. Natl Acad. Sci. USA* **107**, 12941–12945 (2010).
20. Deutsch, C., Brix, H., Ito, T., Frenzel, H. & Thompson, L. Climate-forced variability of ocean hypoxia. *Science* **333**, 336–339 (2011).
21. Dell, A. I., Pawar, S. & Savage, V. M. Systematic variation in the temperature dependence of physiological and ecological traits. *Proc. Natl Acad. Sci. USA* **108**, 10591–10596 (2011).
22. Verberk, W. C. E. P., Bilton, D. T., Calosi, P. & Spicer, J. I. Oxygen supply in aquatic ectotherms: partial pressure and solubility together explain biodiversity and size patterns. *Ecology* **92**, 1565–1572 (2011).
23. Emerson, S. & Hedges, J. *Chemical Oceanography and the Marine Carbon Cycle* (Cambridge Univ. Press, 2008).
24. Kristensen, E. Ventilation and oxygen uptake by three species of *Nereis* (Annelida: Polychaeta). II. Effects of temperature and salinity changes. *Mar. Ecol. Prog. Ser.* **12**, 229–306 (1983).
25. Gehrke, P. C. Response surface analysis of teleost cardio-respiratory responses to temperature and dissolved oxygen. *Comp. Biochem. Physiol. A* **89**, 587–592 (1988).
26. Spitzer, K. W., Marvin, D. E. Jr & Heath, A. G. The effect of temperature on the respiratory and cardiac response of the bluegill sunfish to hypoxia. *Comp. Biochem. Physiol.* **30**, 83–90 (1969).
27. Kielland, Ø. N., Bech, C. & Einum, S. Warm and out of breath: thermal phenotypic plasticity in oxygen supply. *Funct. Ecol.* **33**, 2142–2149 (2019).
28. Chung, M.-T., Trueman, C. N., Godiksen, J. A., Holmstrup, M. E. & Grønkjær, P. Field metabolic rates of teleost fishes are recorded in otolith carbonate. *Commun. Biol.* **2**, 24 (2019).
29. Pörtner, H.-O. Oxygen- and capacity-limitation of thermal tolerance: a matrix for integrating climate-related stressor effects in marine ecosystems. *J. Exp. Biol.* **213**, 881–893 (2010).
30. Verberk, W. C. E. P., Durance, I., Vaughan, I. P. & Ormerod, S. J. Field and laboratory studies reveal interacting effects of stream oxygenation and warming on aquatic ectotherms. *Glob. Change Biol.* **22**, 1769–1778 (2016).
31. Verberk, W. C. E. P., Leuven, R. S. E. W., van der Velde, G. & Gabel, F. Thermal limits in native and alien freshwater peracarid Crustacea: the role of habitat use and oxygen limitation. *Funct. Ecol.* **32**, 926–936 (2018).
32. Sunday, J. M., Bates, A. E. & Dulvy, N. K. Thermal tolerance and the global redistribution of animals. *Nat. Clim. Change* **2**, 686–690 (2012).
33. Verberk, W. C. E. P. et al. Does oxygen limit thermal tolerance in arthropods? A critical review of current evidence. *Comp. Biochem. Physiol. A* **192**, 64–78 (2016).
34. Lefevre, S. Are global warming and ocean acidification conspiring against marine ectotherms? A meta-analysis of the respiratory effects of elevated temperature, high $CO_2$ and their interaction. *Conserv. Physiol.* **4**, cow009 (2016).
35. Jutfelt, F. et al. Oxygen- and capacity-limited thermal tolerance: blurring ecology and physiology. *J. Exp. Biol.* **221**, jeb169615 (2018).
36. Ern, R., Norin, T., Gamperl, A. K. & Esbaugh, A. J. Oxygen dependence of upper thermal limits in fishes. *J. Exp. Biol.* **219**, 3376–3383 (2016).
37. Deutsch, C. A. et al. Impacts of climate warming on terrestrial ectotherms across latitude. *Proc. Natl Acad. Sci. USA* **105**, 6668–6672 (2008).
38. Sunday, J. M. et al. Thermal-safety margins and the necessity of thermoregulatory behavior across latitude and elevation. *Proc. Natl Acad. Sci. USA* **111**, 5610–5615 (2014).
39. Rummer, J. L. et al. Life on the edge: thermal optima for aerobic scope of equatorial reef fishes are close to current day temperatures. *Glob. Change Biol.* **20**, 1055–1066 (2014).
40. Penn, J. L., Deutsch, C., Payne, J. L. & Sperling, E. A. Temperature-dependent hypoxia explains biogeography and severity of end-Permian marine mass extinction. *Science* **362**, eaat1327 (2018).
41. Killen, S. S. et al. Ecological influences and morphological correlates of resting and maximal metabolic rates across teleost fish species. *Am. Nat.* **187**, 592–606 (2016).

# Methods

## Derivation of the Metabolic Index

The Metabolic Index is defined as per a previous study[4] as the ratio of the rates of the $O_2$ supply to and demand by an organism. In general, both rates are dependent on temperature ($T$) and body mass ($B$). Following standard metabolic scaling, the $O_2$ demand can be written:

$$D = \alpha_D B^\delta \exp\left\{\frac{-E_d}{k_B}\left(\frac{1}{T} - \frac{1}{T_{ref}}\right)\right\}, \qquad (2)$$

where the rate coefficient ($\alpha_D$) has units of $O_2$ per unit body mass per time (we use $\mu$mol $O_2\,g^{-3/4}\,h^{-1}$). It is scaled by the exponential Arrhenius function of absolute temperature, which captures the temperature dependence often described by a Q10 factor[42]. When estimating parameters, the body mass is normalized to the median experimental body mass so that it is non-dimensional. Thus, when $T = T_{ref}$, an organism of median body mass has a resting metabolic rate of $D = \alpha_D$.

The supply of $O_2$ to the body may also scale with body size, temperature and ambient $O_2$ pressure ($p_{O_2}$), such that:

$$S = \hat{\alpha}_S(T)B^\sigma p_{O_2} \qquad (3)$$

The function $\hat{\alpha}_S(T)$ represents the efficacy of the $O_2$ supply. It is a rate coefficient (in $\mu$mol $O_2\,g^{-3/4}\,h^{-1}\,atm^{-1}$), but becomes an absolute mass-normalized rate ($\mu$mol $O_2\,g^{-3/4}\,h^{-1}$) only when multiplied by the ambient $O_2$ pressure (we use units of atm). The exponent, $\sigma$, for the allometric scaling of the $O_2$ supply with body mass is typically very similar to that of $O_2$ demand[18], although the two may differ.

The temperature dependence of $\hat{\alpha}_S(T)$ may be complicated, as it reflects the combined effect of multiple steps in the $O_2$ supply chain, including ventilation and circulation rates that are under biological control, as well as diffusive $O_2$ flux across the water–body boundary. Because diffusive gas fluxes are governed by physical and chemical kinetics, their temperature dependence follows the known scaling of gas exchange across a diffusive boundary layer[43]. Standard gas exchange models are well approximated by an Arrhenius function (Extended Data Fig. 3a):

$$\hat{\alpha}_S(T) = \alpha_S \exp\left\{\frac{-E_S}{k_B}\left(\frac{1}{T} - \frac{1}{T_{ref}}\right)\right\} \qquad (4)$$

where the scalar coefficient $\alpha_S$ has the same units as the function $\hat{\alpha}_S(T)$, but is a constant that does not depend on temperature. The same equation can be applied to ventilation rates and circulation rates, although in contrast to diffusion, for biological rates a single $E_S$ value will not necessarily apply over the entire temperature range of a species (Extended Data Fig. 3b). Even so, equation (4) provides a flexible formula for biological fluxes that vary nonlinearly with temperature over a finite temperature range.

Inserting equations (2)–(4) into the definition of the Metabolic Index, we get:

$$\Phi = \frac{S(B, T, p_{O_2})}{D(B, T)} = \frac{1}{V_h} B^\varepsilon p_{O_2} \exp\left\{\frac{E_o}{k_B}\left[\frac{1}{T} - \frac{1}{T_{ref}}\right]\right\} \qquad (5)$$

where

$$\varepsilon = \sigma - \delta, \qquad (6a)$$

$$E_o = E_d - E_S \qquad (6b)$$

and

$$V_h = \alpha_D/\alpha_s \qquad (6c)$$

The defining formula (equation (5)) is identical to equation (1) in the main text, and to the previously described formula given by ref. [4]. It differs in form from that described previously[4] because it is normalized to a reference temperature ($T_{ref}$) such that when $T = T_{ref}$ (here specified at 15 °C), the coefficient ($\alpha_S/\alpha_D = 1/V_h$, which is denoted $A_o$ in the previous study[4]) is the inverse of $P_{crit}$ at that reference temperature. We have also chosen a more intuitive annotation for the allometric exponents ($\sigma$, for 'supply' and $\delta$, for 'demand'). The only substantial difference in this formulation is that the contributions of the $O_2$ supply and demand to the temperature sensitivity of hypoxia tolerance (that is, $E_o$) are made explicit, rather than being accounted for implicitly (for example, see supplementary figure 2 of the previous study[4]). This allows the net temperature dependence of the tolerance of hypoxia to be partitioned into supply and demand effects using equations (6a)–(6c).

## Data compilation and parameter estimation

The physiological parameters of the Metabolic Index ($\Phi$) are derived from laboratory measurements of hypoxic thresholds ($P_{crit}$) and resting metabolic rates ($D$) at multiple temperatures. The measurements are taken from published literature, adding to previous compilations[7,40,44]. The original studies and parameter values are listed in Supplementary Table 1, and yield 145 species with metabolic rate parameters, and 72 species with hypoxia parameters (including four based on lethal thresholds ($LC_{50}$)). The species with $P_{crit}$ data range over 8 orders of magnitude in body mass, from 5 phyla (Annelida, Arthropoda, Chordata, Cnidaria and Mollusca), including 31 malacostracans, 26 fishes, 9 molluscs, 2 copepods, and 1 species each for ascidians, thaliaceans, scleractinian corals and annelid worms.

Metabolic traits ($\delta$, $\alpha_D$, $E_d$) are derived from fitting equation (2) with mass-normalized resting metabolic rates ($\mu$mol $O_2\,h^{-1}g^{-3/4}$) that have been experimentally determined at multiple temperatures. Hypoxia traits ($\varepsilon$, $V_h$ and $E_o$) are derived by substituting paired experimental temperatures and $P_{crit}$ data (atm) in equation (5) (as variables $T$ and $p_{O_2}$), and solving for the parameters that give $\Phi = 1$, the condition in which the physical $O_2$ supply and resting metabolic demand are balanced. Parameters describing the net $O_2$ supply ($\alpha_S$ and $E_S$) were estimated from equations (6a)–(6c), that is, $\alpha_S = \alpha_D/V_h$ and $E_S = E_d - E_o$, for the subset of species for which $P_{crit}$ and metabolic rates are both available at multiple temperatures. The temperature dependence of the net $O_2$ supply is compared to independent estimates based on the individual steps in the $O_2$ supply chain: diffusion, ventilation and circulation (Extended Data Fig. 3). With species for which body mass varied by less than a factor of 2, we set $\delta = 3/4$ and $\varepsilon = 0$, values that typify most species, including those investigated here.

We analysed the parameters of the Metabolic Index in two complementary ways. First, we compare the interspecies frequency distributions of each parameter, which emphasizes the diversity of traits and their relationships across marine biota, and enables comparisons between traits that are not all measured in all species. Second, we examine the intraspecies relationships between traits whenever multiple traits from the same species are available. Such analyses provide a more direct test of physiological mechanisms, but are taxonomically restricted and more sensitive to random errors in the experimental determination of parameters.

We use MATLAB's nonlinear fitting routine (fitnlm.m) to solve for species traits (parameters) that minimize the squared residual errors. We report the central estimate of each parameter, the Pearson correlation coefficient ($r^2$) and the $P$ value based on two-sided Student's $t$-tests, and the number of raw observations in Supplementary Table 1. With species parameters obtained from equations (1), (2), (6), relationships between traits are subsequently analysed using a standard linear least squares MATLAB routine (regress.m). Regression parameters, their 95% confidence intervals, correlation coefficients ($r^2$), the $P$ value based on two-sided $t$-tests and the number of raw observations for each relationship are reported in Extended Data Table 1.

# Article

To maximize the number of species analysed, we include those for which experiments were conducted at as few as 2 temperatures. However, all reported relationships among traits were confirmed using the subset of species ($n = 14$) for which regressions of metabolic rates and $P_{crit}$ data against temperature were statistically significant ($P < 0.05$, two-tailed $t$-test) (Extended Data Fig. 2).

## Determination and validation of $\Phi_{crit}$

The limiting value of the Metabolic Index in each species habitat ($\Phi_{crit}$), was estimated by pairing species location data with hydrographic conditions at those locations. Occurrence data were downloaded from the Ocean Biodiversity Information System (OBIS; http://iobis.org) in September 2019. Of the 72 species with hypoxia traits, OBIS contains georeferenced presence data for 68. To estimate the hydrographic conditions at each specimen location, we used monthly climatological temperature and $O_2$ fields at a resolution of 1° latitude and longitude and at 33 depths from the World Ocean Atlas[45,46]. For analysis of temperature at the sea surface ($z = 0$ m) (Fig. 5), we include the diurnal temperature range from satellite remote sensing (data downloaded from https://www.ghrsst.org/ghrsst-data-services/products/) to estimate the globally resolved peak daytime surface temperatures.

Species occurrences were paired to hydrographic data by binning them to the World Ocean Atlas grid for every month based on the locations provided in OBIS. Hydrographic conditions were determined at the central depth of the minimum and maximum depths reported by OBIS, or from either depth alone if only one metric was provided. Occurrences were discarded if the range of conditions within that depth range differed from the central estimate by more than 2 °C for temperature or 20% for $O_2$. For occurrences that did not have depth information altogether, we assigned a minimum depth at the sea surface and maximum depth at the seafloor[47]. In cases in which even this maximum uncertainty in depths satisfied the error tolerance (2 °C for temperature and 20% for $O_2$) the location data were retained. The Metabolic Index (that is, equation (5)) was computed based on species-specific traits and the paired hydrographic data for the occupied sites of each species.

Of the more than 1.5 million OBIS occurrences used here, only 0.1% mapped to climatological conditions in which $\Phi$ falls below 1. This environmental condition is physiologically unsustainable, yet may arise from transient species movements, or a mismatch between the climatological temperature and $O_2$ fields used to compute $\Phi$ and the true in situ hydrographic conditions at the time occurrence data were recorded. Only three species in our dataset had more than 5% of OBIS occurrences for which $\Phi < 1$, and two of them (*Sergia tenuiremis* and *Sergia fulgens*) are known to be vertical migrators. Because of the likelihood that these occurrences do not reflect viable long-term habitats, but instead are being used as a temporary refuge that requires metabolic suppression, we report the $\Phi_{crit}$ values that do not include such locations. Of the three species with more than 5% of locations that had $\Phi < 1$, the removal of those points affected the estimate $\Phi_{crit}$ by <0.3 for two of them (*S. fulgens* and *M. pammelas*), and thus has a negligible effect on our results. We report the $\Phi_{crit}$ estimates both with and without the inclusion of rare locations for which $\Phi < 1$ (Supplementary Table 1).

We evaluated the $\Phi$ value that best defines the boundary of the geographical range of each species in two independent methods, which use identical data but differ in the degree of data aggregation over space and time. The first equates $\Phi_{crit}$ with the lower tail in the frequency distribution of $\Phi$ across all occupied sites in OBIS, for each species. The second computes the $\Phi$ value that maximizes its predictive skill in segregating inhabited and uninhabited grid cells globally, using a machine-learning technique. The two methods, which are described below, give highly consistent results (Extended Data Fig. 8a), but the first approach is presented in the main text (Fig. 4), owing to its conceptual and computational simplicity.

**Occurrence histogram.** The ecological parameter, $\Phi_{crit}$, is estimated from the cumulative distribution function as the value of $\Phi$ above which the most of the occurrences of each species are found (5th and 10th percentiles). The two values yield similar $\Phi_{crit}$ values, and their range encompasses the $\Phi_{crit}$ derived from a machine-learning algorithm (see 'The $F_1$-score'; Extended Data Fig. 8a), but can be applied objectively to species for which the three-dimensional distribution is too complex or sparsely sampled to identify a clear boundary to the geographical range. We present the median of $\Phi_{crit}$ in our primary results, but include both values in Supplementary Table 1.

As sampling density decreases, the lowest observed $\Phi$ value may not reflect the true minimum within a species habitat. However, we found that the distribution of $\Phi_{crit}$ for all species was similar regardless of sampling intensity (Extended Data Fig. 8b), and not biased towards higher values of $\Phi_{crit}$ (Fig. 4). We therefore did not restrict the analysis based on the number of occurrences.

**The $F_1$-score.** We evaluated the ability of $\Phi$ to separate the ocean into inhabited and uninhabited portions for each species, using a standard statistical categorization metric, the $F_1$-score[48,49]. The $F_1$-score is computed based on the presence and absence of a species on a regular grid (latitude, longitude, depth and month), for which the environmental conditions fall above and below a threshold value, which we varied. The value of the environmental threshold that yields the maximum $F_1$-score is the one that best segregates global grid cells into inhabited and uninhabited conditions for the environmental parameter of interest. $\Phi_{crit}$ is estimated as the $\Phi$ value that optimizes the predictive skill of categorizing habitat (maximum $F_1$-score).

The $F_1$-score is calculated as the harmonic mean of precision and recall, with equal weighting given to both measures. Precision measures the probability that the presence of the species in waters for which $\Phi \geq \Phi_{crit}$ is a true positive (TP; specimen reported in the space in which they are predicted to occur) rather than a false positive (FP; specimen reported in a space predicted to be below the $\Phi$ threshold). Recall is the probability that a specimen is actually reported where $\Phi > \Phi_{crit}$ (that is, how likely is a true positive relative to a false negative (FN; missing observations above $\Phi_{crit}$). In terms of these variables, the $F_1$-score can be expressed as:

$$F_1 = \left( \frac{\text{recall}^{-1} + \text{precision}^{-1}}{2} \right)^{-1} = \frac{2\text{TP}}{2\text{TP} + \text{FN} + \text{FP}} \qquad (7)$$

This metric does not give weight to true absence data (species known to be not present), which are infrequently and inconsistently reported in marine species data. It is thus well suited to categorization problems based on OBIS data. A model with perfect precision and recall would have $F_1 = 1$. The absolute $F_1$-score cannot be meaningfully compared between species, as it depends on the total number of grid cells included, as well as the total number of occupied sites. However, when applied to the same species and geographical region, the variations in $F_1$-scores between different values of the same environmental parameter, or between different environmental parameters (for example, $\Phi$ versus $T$), are a meaningful metric for the relative skill of a given parameter and its threshold value. Optimal $F_1$-scores were used to compare the predictive skill of different environmental parameters.

**Comparison to SMS.** To determine whether $\Phi_{crit}$ is consistent with independent estimates of the ratio of active-to-resting metabolic rates, we compared the frequency distributions of both metrics. An appropriate direct comparison of the habitat constraint ($\Phi_{crit}$) to metabolic rate ratios would be based on active metabolic rates sustained over the time scales of population maintenance (termed 'SusMR')[8]. Such rates are not measured in marine species. However, maximum rates

of metabolism are commonly measured in laboratory experiments. Long-term sustained metabolic rates can be expressed as a weighted average of the maximum rates (MMR) obtained under extreme exertion and the minimum rates that apply in a state of rest (RMR):

$$\text{SusMR} = w_R \times \text{RMR} + (1 - w_R) \times \text{MMR}$$

where $w_R$ represents the effective weight of the resting state in the time–mean sustained metabolic rate. Dividing both sides by RMR, and noting the definition of SMS (SMS = SusMR/RMR), yields the equation in the main text:

$$\text{SMS} = w_R + (1 - w_R)(\text{MMR/RMR}), \tag{8}$$

which can be rearranged, substituting the definition of factorial aerobic scope (FAS = MMR/RMR) to estimate the weighting factor, $w_R$:

$$w_R = \frac{\text{FAS} - \text{SMS}}{\text{FAS} - 1}. \tag{9}$$

Carbon isotope analyses of the otoliths of Atlantic Cod[22] suggest that SMS ≈ 2, whereas FAS[50] ranges from 3.3 to 3.8, yielding a range of $w_R$ from 0.39 to 0.47. We estimated the weighting of resting metabolic rates (that is, $w_R$) using the measured ratios of MMR/RMR and $\Phi_{crit}$ for the species in our dataset (Supplementary Table 1), and find a mean and interspecies variation (s.d.) ($w_R = 0.40 \pm 0.17$, $n = 14$; Extended Data Fig. 9 and Supplementary Table 1) that is consistent with the direct geochemical estimate for cod. Extending the mean value from these 14 species to a broader group of species with measured FAS[41] ($n = 106$) but no SMS or $\Phi_{crit}$, we find a distribution of SMS that is statistically indistinguishable from the overall distribution of $\Phi_{crit}$ (Extended Data Table 1). Interspecies variation in the estimates of $w_R$ probably reflects both real biological differences in activity levels and the substantial methodological uncertainties that originate from both laboratory rates (MMR and RMR) and biogeographically derived $\Phi_{crit}$ values. Regardless of the precise values of $w_R$ and their uncertainties, the fact that they are all positive (FAS values are at or above $\Phi_{crit}$) and that $\Phi_{crit}$ is significantly correlated with laboratory-derived SMS and MMR/RMR measurements (Extended Data Table 1 and Extended Data Fig. 9) indicates that aerobic energy availability is a habitat constraint.

**Estimation of AT$_{max}$.** The maximum temperature at which aerobic respiration can be sustained is estimated by extrapolating the empirical relationship between $P_{crit}$ and temperature to the mean atmospheric $p_{O_2}$ ($P_{atm}$), at which CT$_{max}$ experiments are carried out. We thus find the solution to the equation:

$$A_o P_{atm} \exp\left\{ \frac{E_o}{k_B}\left[ \frac{1}{\text{AT}_{max}} - \frac{1}{T_{ref}} \right]\right\} = \begin{cases} 1 & \text{resting AT}_{max} \\ \Phi_{crit} & \text{active AT}_{max} \end{cases} \tag{10}$$

Because the $P_{crit}$ data are all below $P_{atm}$, the solutions to this equation (AT$_{max}$) are necessarily extrapolated beyond the experimental range of temperatures over which $E_o$ is estimated. If $E_o$ was constant across the full range of temperatures, this extrapolation would only be influenced by the random errors in $P_{crit}$ measurements, but would not incur a systematic bias across all species, yielding a histogram of AT$_{max}$ with a robust mean value. However, the available data indicate that $E_o$ increases systematically (albeit slightly) with temperature (Extended Data Fig. 3). We correct for this bias in the extrapolation of $P_{crit}$ curves to the aerobic thermal maximum, by including an empirically derived linear increase in $E_o$ with temperature, as discussed next.

The slope of the relationship (denoted by the derivative of $E_o$ with respect to temperature, $dE_o/dT$) is estimated in multiple ways, to evaluate the uncertainty in these extrapolations. First, we use the intraspecies difference in $E_o$ among species for which it can be separately estimated both above and below $T_{ref}$, as discussed in the main text and shown in Extended Data Fig. 3. This yields a mean intraspecies $dE_o/dT = 0.036$ eV/°C (0.55 eV/15 °C, where 15 °C is the difference between the two temperature bins 0–15 °C and 15–30 °C). Second, we consider the differences in $E_o$ between colder waters ($T < T_{ref}$) and warmer waters ($T > T_{ref}$) for all species. This estimate, $dE_o/dT = 0.013$ eV/°C (0.2 eV/15 °C; Extended Data Fig. 3) gives a lower value because it includes interspecies variation. Finally, as a third method for estimating the potential variation in $E_o$ with temperature, we directly fit the $P_{crit}$ curves (equation (5) for all species with more than 2 temperatures, including a linear relationship between $E_o$ and temperature. We discard any fits that predict a $P_{crit}$ that declines towards zero at high temperatures ($T \gg 30$ °C), as this would imply an unrealistic (infinite) tolerance for hypoxia at high temperatures. As a second check on the curve fits, we compare the Akaike information criterion (AIC) for the model with a linear increase in $E_o$ to our standard model with a constant $E_o$. We only retain those curve fits in which the AIC did not decrease, indicating that the additional parameter did not reduce the information content of the model despite the additional parameter. Across species, this yields a mean value of $dE_o/dT = 0.022$ eV/°C, which falls in between the previous two values. We apply this interspecies mean value as a default value for all species (Fig. 5), since it yields results that are not biased relative to values derived from species-specific $dE_o/dT$ wherever both are available (Extended Data Fig. 10). The range of $dE_o/dT$ estimates is used to generate the error bars of the estimates of AT$_{max}$ plotted in Extended Data Fig. 10.

### Reporting summary

Further information on research design is available in the Nature Research Reporting Summary linked to this paper.

## Data availability

The data used in this study are described in the Methods. The data that support the findings of this study are available from the corresponding author upon reasonable request.

## Code availability

The MATLAB code is available at GitHub (https://github.com/cadeutsch/Metabolic-Index-Traits).

42. Gillooly, J. F., Brown, J. H., West, G. B., Savage, V. M. & Charnov, E. L. Effects of size and temperature on metabolic rate. *Science* **293**, 2248–2251 (2001).
43. Malte, H. & Weber, R. E. A mathematical model for gas exchange in the fish gill based on non-linear blood gas equilibrium curves. *Respir. Physiol.* **62**, 359–374 (1985).
44. Rogers, N. J., Urbina, M. A., Reardon, E. E., McKenzie, D. J. & Wilson, R. W. A new analysis of hypoxia tolerance in fishes using a database of critical oxygen level ($P_{crit}$). *Conserv. Physiol.* **4**, cow012 (2016).
45. Locarnini, R. A. et al. *World Ocean Atlas 2013. Volume 1: Temperature* (National Centers for Environmental Information, National Oceanic and Atmospheric Administration, 2013).
46. Garcia, H. E. et al. *World Ocean Atlas 2013, Volume 3: Dissolved Oxygen, Apparent Oxygen Utilization, and Oxygen Saturation* (National Centers for Environmental Information, National Oceanic and Atmospheric Administration, 2013).
47. Amante, C. & Eakins, B. W. *ETOPO1 1 Arc-Minute Global Relief Model: Procedures, Data Sources and Analysis.* NOAA Technical Memorandum NESDIS NGDC-24 https://doi.org/10.7289/V5C8276M (2009).
48. Shawe-Taylor, J. & Cristianini, N. *Kernel Methods for Pattern Analysis* (Cambridge Univ. Press, 2004).
49. Liu, C., White, M. & Newell, G. Measuring and comparing the accuracy of species distribution models with presence–absence data. *Ecography* **34**, 232–243 (2011).
50. Schurmann, H. & Steffensen, J. F. Effects of temperature, hypoxia and activity on the metabolism of juvenile Atlantic cod. *J. Fish Biol.* **50**, 1166–1180 (1997).
51. Heath, A. G. & Hughes, G. M. Cardiovascular and respiratory changes during heat stress in rainbow trout (Salmo gairdneri). *J. Exp. Biol.* **59**, 323–338 (1973).

# Article

**Extended Data Fig. 1 | Species metabolic rates and hypoxia tolerances from laboratory studies. a, b**, Measured metabolic rates (μmol g$^{-1}$ h$^{-1}$) (**a**) and critical O$_2$ pressures ($P_{crit}$) (**b**) versus temperature (°C) in published laboratory experiments (circles). For clarity, metabolic rates are shown only for the subset of species with $P_{crit}$ data. **c**, Location data from OBIS for all species with $P_{crit}$ measured at multiple temperatures, yielding calibrated Metabolic Index parameters. The number of species with occurrences in the Pacific, Atlantic and Indian Oceans are labelled. Maps of the occurrences of individual species are available at https://obis.org/.
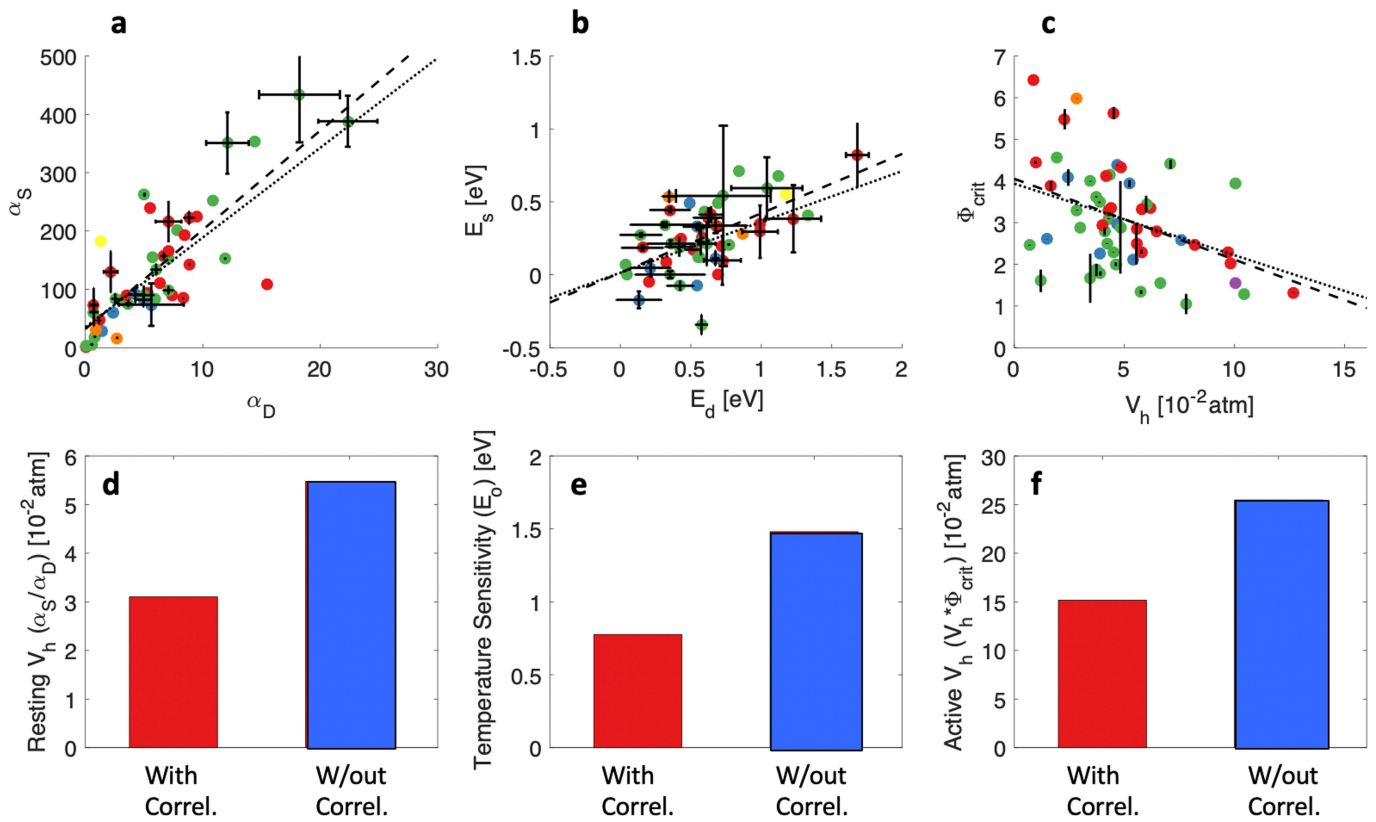
**Extended Data Fig. 2 | Correlations and diversity in traits that govern geographical range boundaries. a–c,** The key traits that make up resting hypoxia vulnerability ($V_h = \alpha_D/\alpha_S$) (**a**), its temperature sensitivity ($E_o = E_d - E_s$) (**b**) and the elevated hypoxia vulnerability under activity ($V_h \times \Phi_{crit}$) (**c**) all exhibit significant correlations (standard linear regression, two-tailed $t$-test, $P < 0.05$) between their constitutive parameters, regardless of whether we use all 72 species (dashed lines) or the subset of 14 species (dotted lines) for which the traits themselves were derived from statistically significant fits to equations (1) and (2) (see Methods and Extended Data Table 1). As in Fig. 1, points and error bars (centred dot, if shorter than marker) are mean ± s.e.m. for species with more than two independent experimental temperatures. See Supplementary Table 1 for the number of independent temperature experiments used for each species. The number of species used in each correlation is $n = 48$ (**a**, **b**) and $n = 56$ (**c**). See Extended Data Table 1 for statistics on two-sided $t$-tests of trait correlations. **d–f,** Observed diversity in resting hypoxia vulnerability ($V_h$) (**d**), its temperature

sensitivity ($E_o$) (**e**) and active hypoxia vulnerability ($V_h \times \Phi_{crit}$) (**f**), is measured as the interquartile range (IQR) among all species (red bars). We also quantified the diversity in species traits in the absence of observed correlations in the underlying metabolic traits. The correlations are removed by replacing species variation in the indicated parameter with the interspecies mean value. The diversity of the resulting trait is recomputed from the IQR (blue bars). Specifically, we replace the variable $\alpha_S$ (**a**) with its mean value to derive a new distribution and IQR of $V_h$ (**d**, blue bar); replace the variable $E_s$ (**b**) with its mean value to derive a new distribution and IQR of $E_o$ (**e**, blue bar) and replace the variable $\Phi_{crit}$ (**c**) with its mean value to derive a new distribution and IQR of the active hypoxia tolerance ($V_h \times \Phi_{crit}$; **f**, blue bar). For all three central traits, the correlation and putative trade-offs among the underlying constitutive parameters act to reduce the interspecies diversity of the trait that governs habitat range limits.
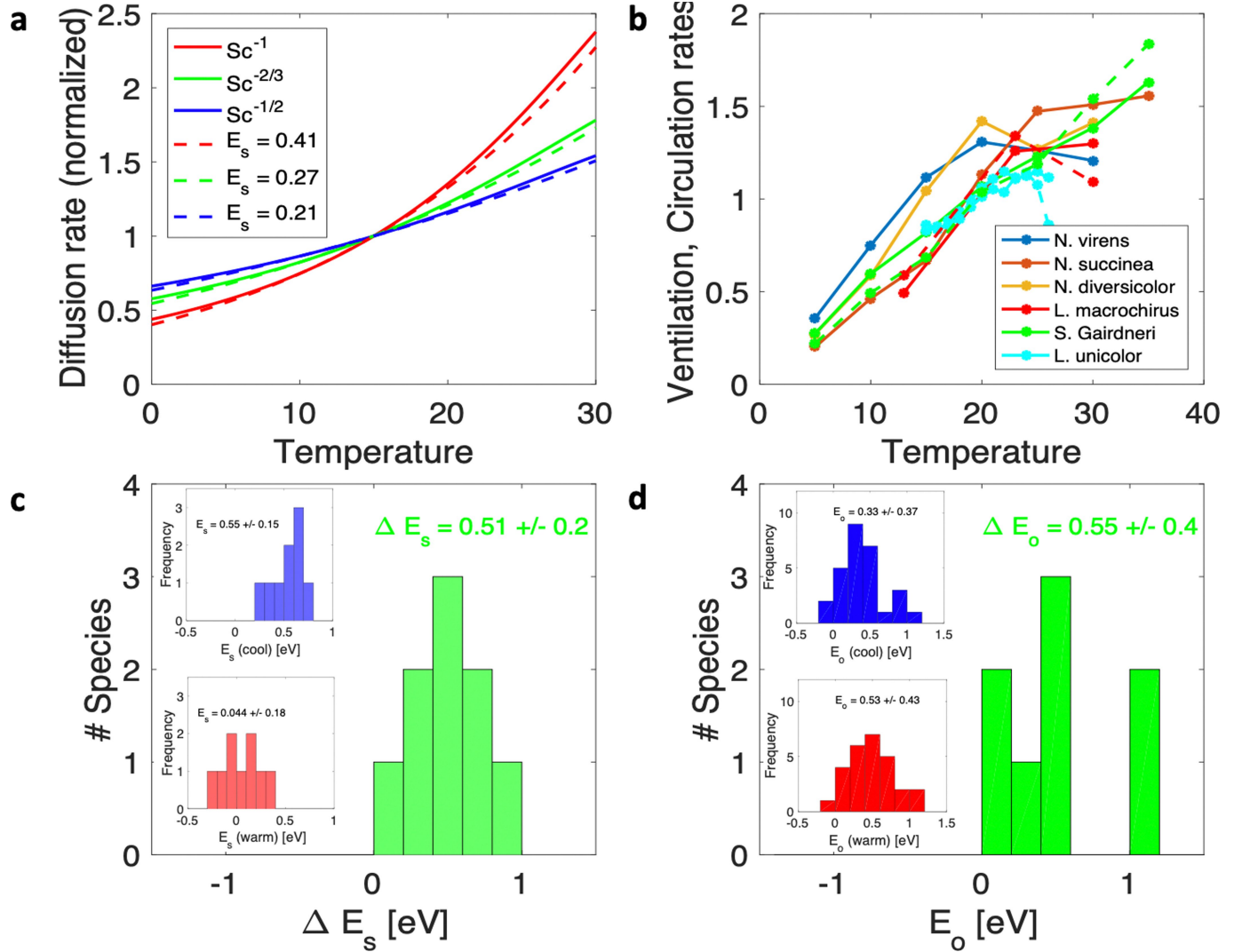
**Extended Data Fig. 3 | Temperature sensitivity of processes that govern the O₂ supply. a**, The rate of diffusive flux across the boundary layer increases with temperature in proportion to $Sc^n$, where the Schmidt number (Sc) is the ratio of seawater viscosity ($v$) to $O_2$ diffusivity ($\kappa$). Typical values of the exponent, $n$, are $-1/2$, $-2/3$ and $-1$, depending on the underlying model of boundary layer renewal[23]. In all cases, the empirically derived curves (solid) are well approximated by an Arrhenius function (dashed) with corresponding activation energy parameters (that is, $E_s$) ranging from 0.21 eV (for $n = -1/2$; blue) to 0.27 eV (for $n = -2/3$; green) and 0.42 eV (for $n = -1$; red). **b**, Experimental measurements of rates of the ventilation (solid) and circulation (dashed) of animals. Rates at multiple temperatures are from published studies of six species, including three annelids[24] (*Nereis virens*, blue; *Nereis succinea*, brown; and *Nereis diversicolor*, gold; all with $n = 6$ independent experiments) and three chordates (*Lepornis macrochirus*[26], red; *Oncorhynchus mykiss*[51], green;

*Leiopotherupon unicolor*[25], cyan; all with $n = 7$ independent experiments). **c**, For each species, the temperature sensitivity of each rate is determined by fitting to an Arrhenius function above and below 20 °C, the approximate thermal midpoint of all data. Histograms of activation energy in each temperature range (insets) are significantly different (two-sample Kolmogorov–Smirnov test; $P = 5 \times 10^{-4}$) for warm conditions ($E_s = 0.04 \pm 0.18$ (mean ± s.d.)) and cool waters ($E_s = 0.55 \pm 0.15$ (mean ± s.d.)). **d**, Distributions of $E_o$ computed from experimental data at temperatures at or above 15 °C (red bars) are higher than for the same parameter computed using only temperatures at or below 15 °C (blue bars). For species for which at least two $P_{crit}$ values were available both above and below $T_{ref}$, the difference between $E_o$ for warm and cold temperatures (green bars) is always greater than zero, and has a mean value (0.55 eV) similar to the change in temperature dependence of ventilation and circulation rates across cold and warm temperatures (green bars in **c**).
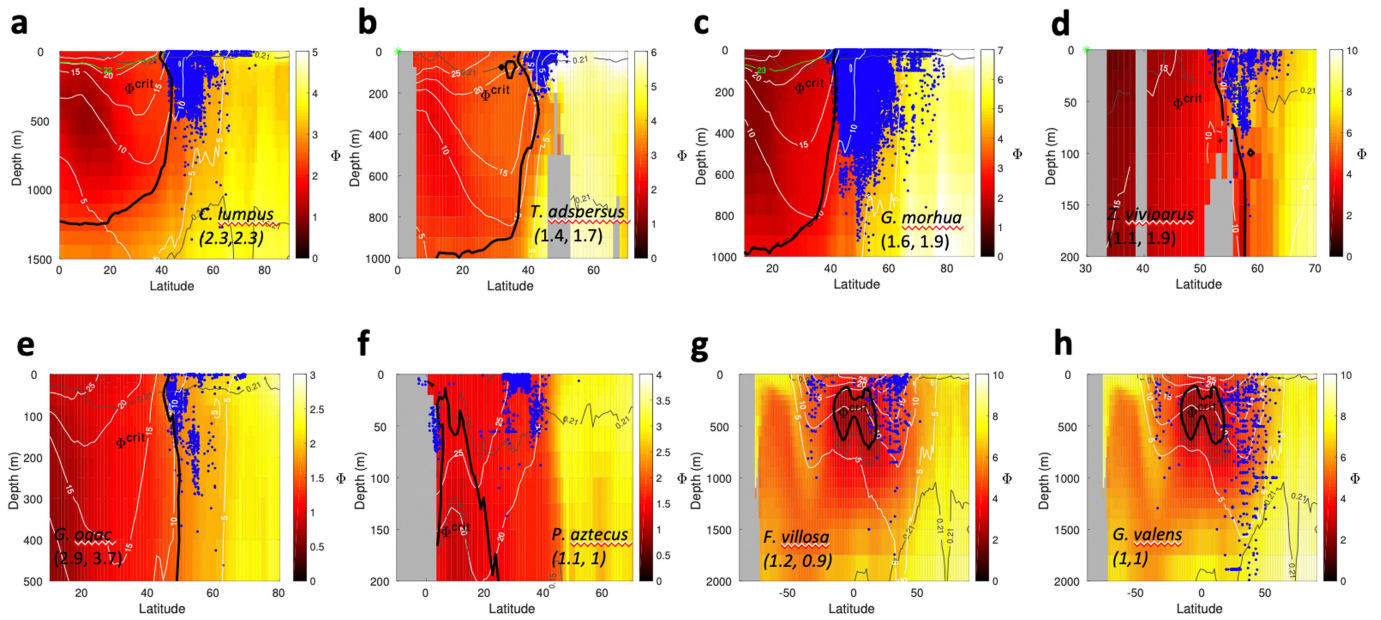
**Extended Data Fig. 4 | Spatial distributions of the Metabolic Index, temperature and $p_{O_2}$ compared to occurrences of species that occupy diverse latitude and depth ranges. a**–**e**, Species inhabit mid to high latitudes. **f**–**h**, Species are found in tropical waters. Fields of $\Phi$ (colours), temperature and $O_2$ pressure are zonally averaged over the longitudinal range of each species. **a**, *Cyclopterus lumpus* (95 °W–35 °E). **b**, *Tautogolabrus adspersus* (50–80 °W). **c**, *Gadus morhua* (75 °W–40 °E). **d**, *Zoarces viviparus* (10 °W–30 °E). **e**, *Gadus ogac* (110 °W–40 °E). **f**, *Penaeus aztecus* (40–120 °W). **g**, *Funchalia villosa* (100 °W–40 °E). **h**, *Gennadas valens* (100 °W–47 °E). Observed species occurrences are plotted (blue dots). A single lower limit of $\Phi$ bounding each species range is contoured ($\Phi_{crit}$; black lines) alongside isotherms of

temperature (white lines; °C) and isopleths of $p_{O_2}$ (grey lines; atm). Published upper thermal limits ($CT_{max}$) are contoured in green where available, based on maximum monthly ocean temperatures (°C). Green asterisks denote species for which $CT_{max}$ occurs above all mapped maximum monthly temperatures. For most species, $\Phi_{crit}$ more skilfully categorizes occupied habitat than either upper temperature limits or lower $p_{O_2}$ considered individually. This skill is shown by the ratio of $F_1$-scores of $\Phi$ relative to temperature or to $p_{O_2}$ (in parentheses, respectively) from the full four-dimensional species distribution. For *G. morhua*, the monthly range of $\Phi_{crit}$ is also mapped (dashed black lines). For *G. ogac*, mapped occurrences, $\Phi$ and water properties are from the Atlantic Ocean only. Land regions are shaded in grey.
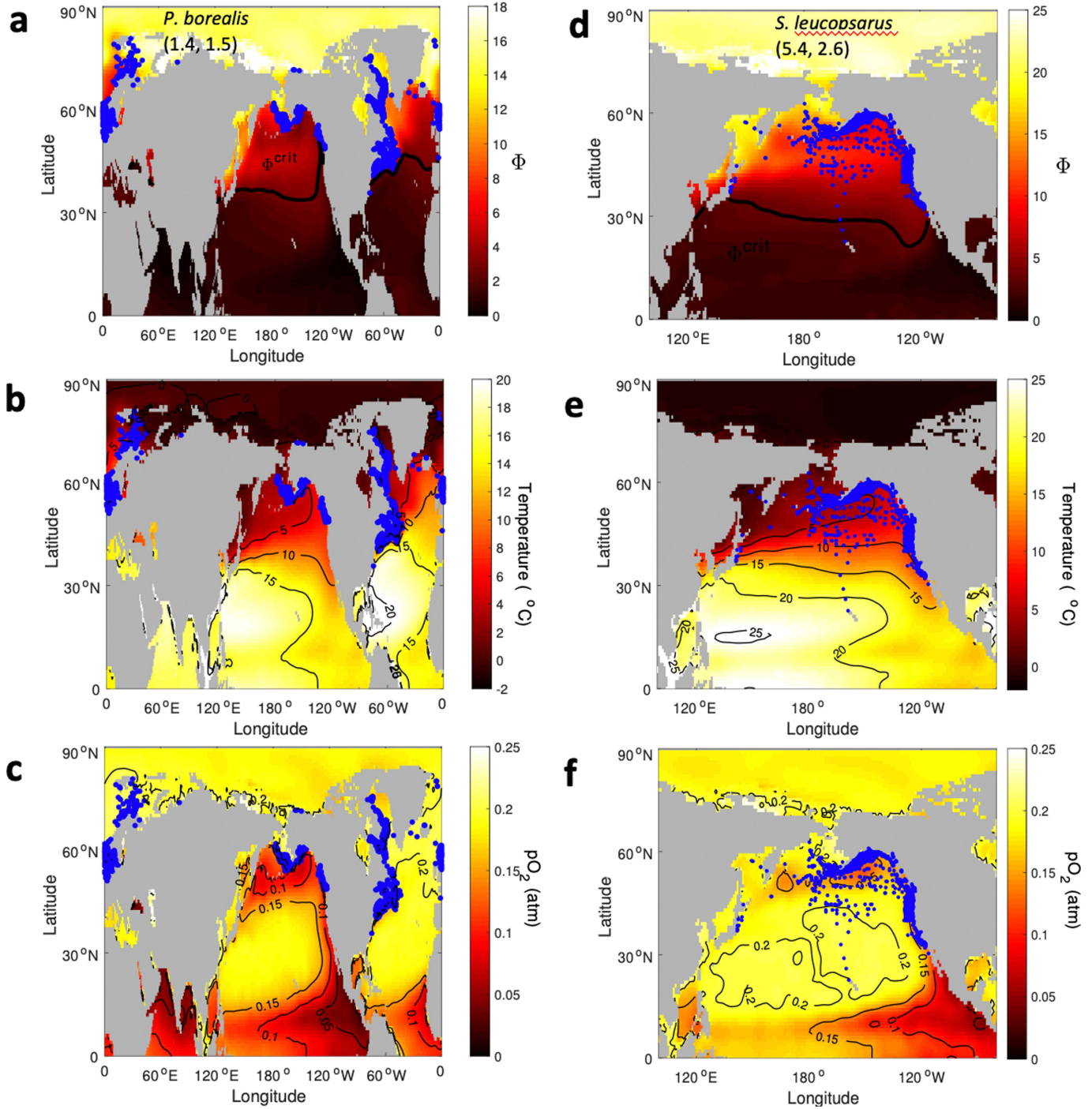
**Extended Data Fig. 5 | Maps of the Metabolic Index, temperature and $p_{O_2}$ compared to species distributions. a–f**, Mapped variables are averaged from the surface to the 95th percentile depth of each species. **a–c**, *P. borealis* (0–450 m). **d–f**, *Stenobrachius leucopsarus* (0–225 m). A single lower limit of $\Phi$ ($\Phi_{crit}$; black lines) is consistent with habitat range limits found in the Pacific and Atlantic Oceans for *P. borealis* (**a**) and different sides of the Pacific Ocean

for *S. leucopsarus* (**d**). By contrast, no single maximum temperature or minimum $p_{O_2}$ is consistent with each species' range limit across those regions. The increased skill of $\Phi_{crit}$ is encapsulated by the higher $F_1$-scores of $\Phi$ relative to temperature (**b**, **e**) or to $p_{O_2}$ (**c**, **f**) (in parentheses, respectively) from the full four-dimensional species distribution. Occurrence data for each species are shown (blue dots).
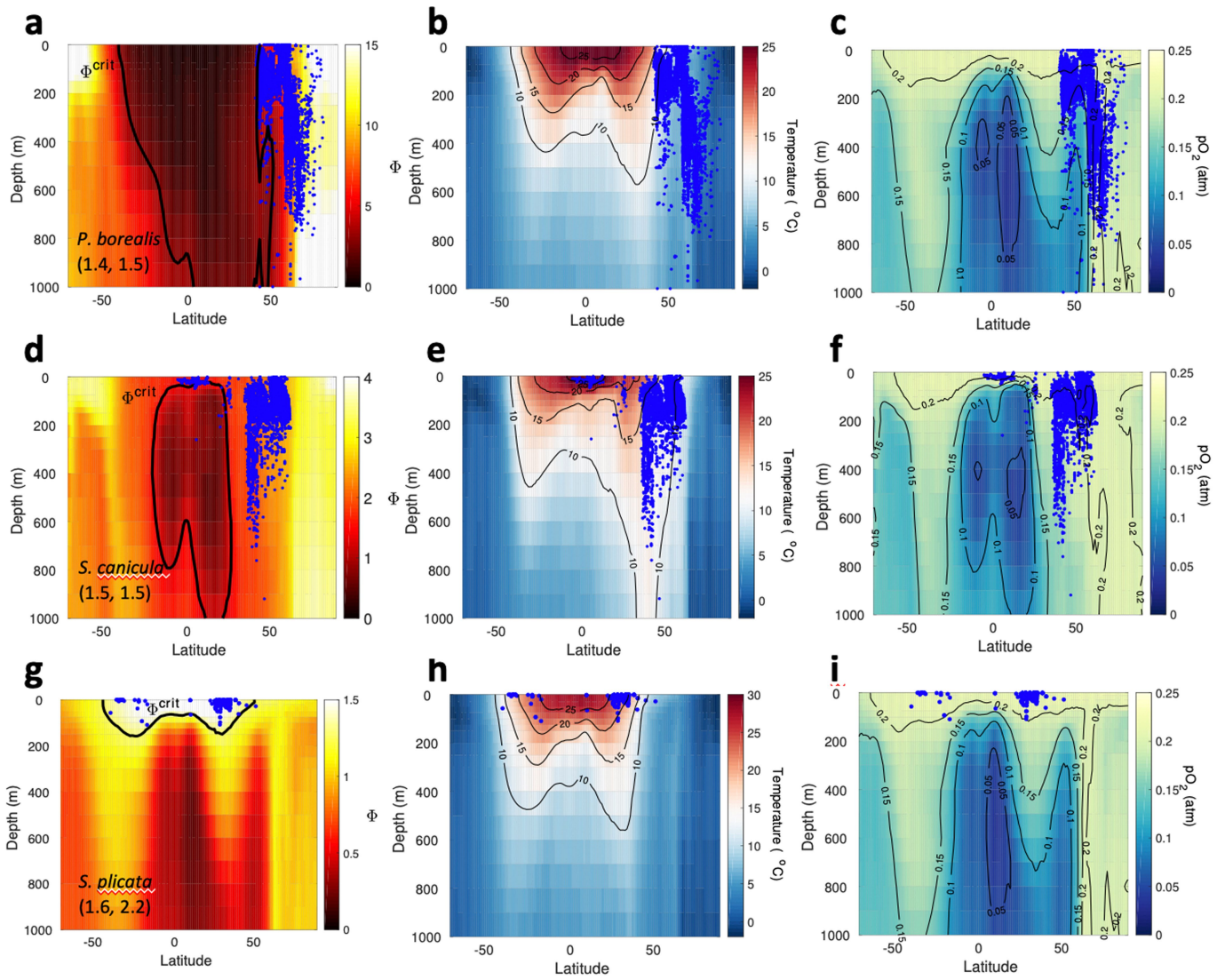
**Extended Data Fig. 6 | Spatial distributions of the *P. borealis*, *S. canicula* and *S. plicata* compared with the Metabolic Index, temperature and $p_{O_2}$.** **a**–**i**, Spatial distributions of the species shown in Fig. 2 (*P. borealis*, *S. canicula* and *S. plicata*) were compared with the Metabolic Index (**a**, **d**, **g**), temperature (**b**, **e**, **h**) and $p_{O_2}$ (**c**, **f**, **i**). **a**–**c**, *P. borealis*. **d**–**f**, *S. canicula*. **g**–**i**, *S. plicata*. A single lower limit of $\Phi$ bounding each species range is contoured ($\Phi_{crit}$; black lines).

For all species, $\Phi_{crit}$ more skilfully categorizes occupied habitat than either temperature limits or lower $p_{O_2}$ considered individually. This skill is shown by the higher ratio of $F_1$-scores of $\Phi$ relative to temperature or to $p_{O_2}$ (in parentheses, respectively) from the full four-dimensional species distribution. Occurrence data for each species are shown (blue dots). Regions for zonal averaging are as in Fig. 2.
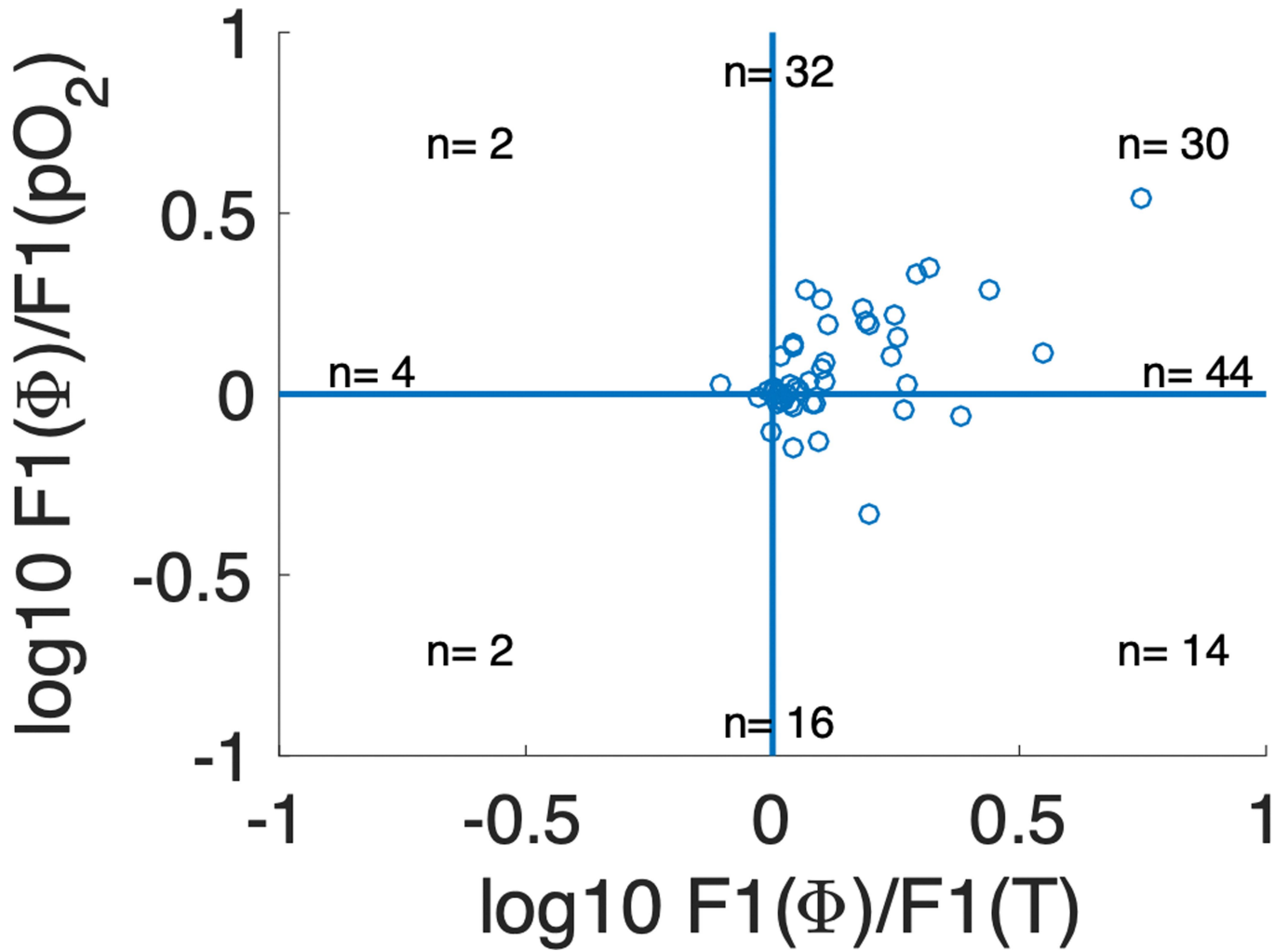
**Extended Data Fig. 7 | Predictive skill of the Metabolic Index in delineating the species geographical range, compared with temperature or $p_{O_2}$ alone.** The $F_1$-score measures the ability of each environmental variable at a given threshold value to categorize the ocean into inhabited and uninhabited regions. The maximum $F_1$-score for $\Phi$ is then compared with the maximum value for temperature or $p_{O_2}$ thresholds and plotted on a $\log_{10}$ scale such that positive (negative) values indicate a stronger (weaker) predictive skill for $\Phi$.

Printed numbers ($n$) on the graph indicate the number of species that fall within each quadrant (for numbers in quadrants) or to each side of the axes (for numbers on axes). For example, $\Phi$ outperforms $T$ in 44 species, and underperforms in only 4, and outperforms both $T$ and $p_{O_2}$ in 30 species. A maximum $F_1$-score was found for 48 species, while 8 additional species had no clear maximum in $F_1$-score.
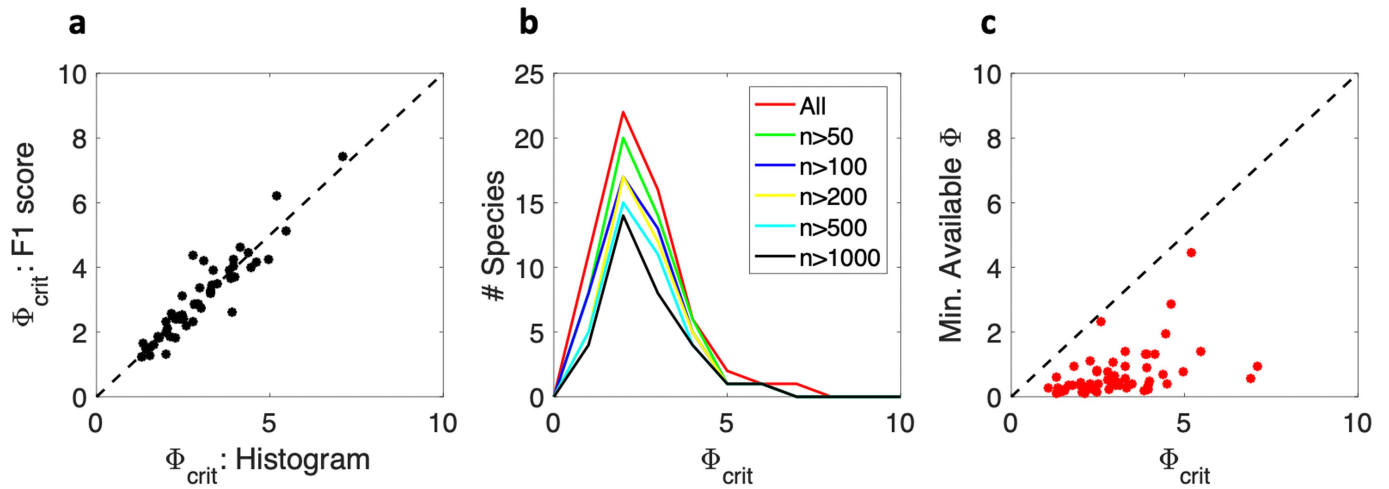
**Extended Data Fig. 8 | Critical value of the Metabolic Index at the limit of species geographical range ($\Phi_{crit}$). a**, The values of $\Phi_{crit}$ are compared using two independent methods. The first ($y$ axis) is determined from the peak in the $F_1$-score for categorization into occupied and unoccupied sites (see Methods). The second ($x$ axis) is determined from the bottom percentile (5–10%) of $\Phi$ values inhabited by the species. **b**, The histogram of $\Phi_{crit}$ is not sensitive to the number of occurrence observations. **c**, For all species, waters with lower $\Phi$ values than $\Phi_{crit}$ exist within the depth range of these species, but lack confirmed specimens. The dashed line indicates the 1:1 line.
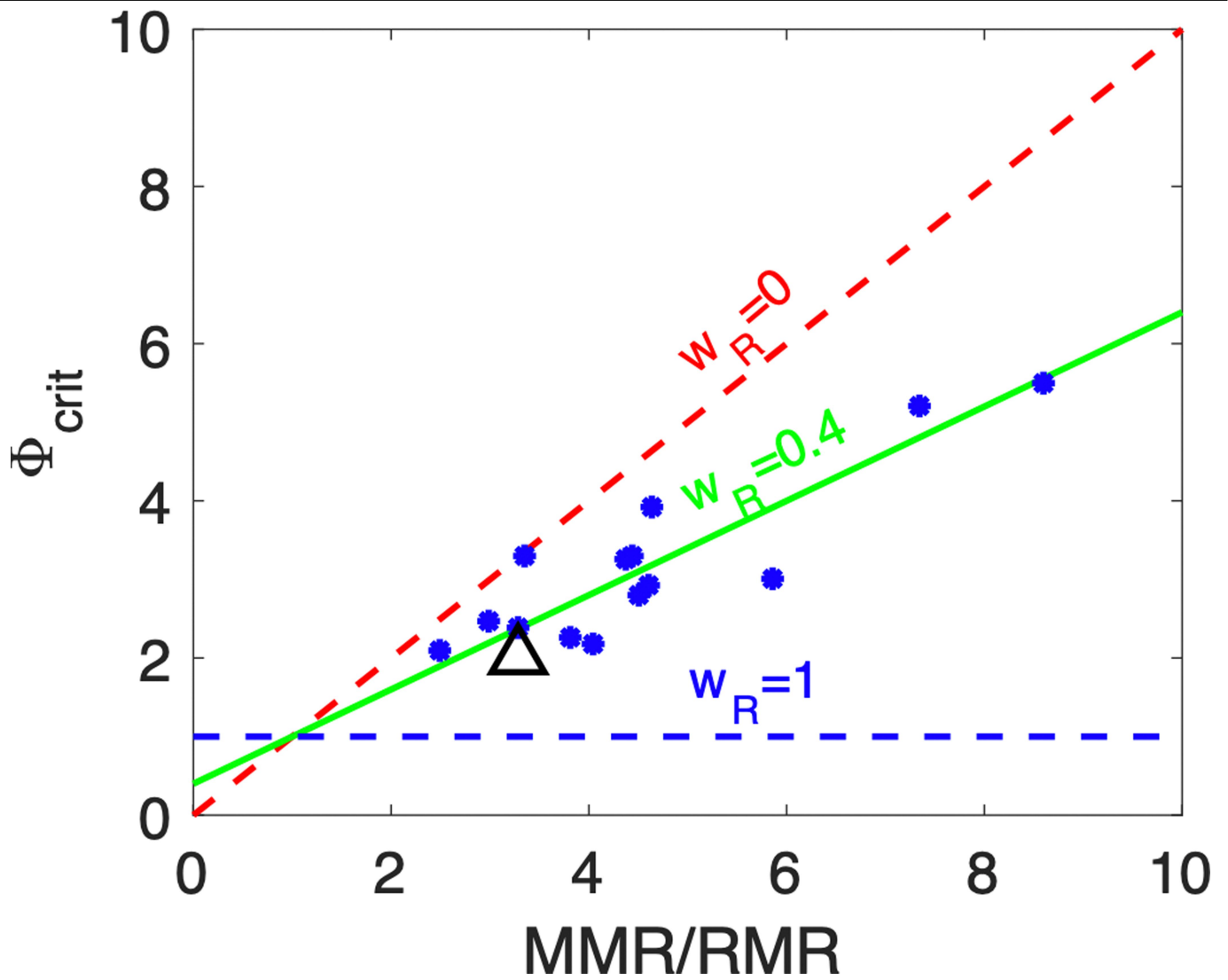
**Extended Data Fig. 9 | Relationship between $\Phi_{crit}$ and the ratio of maximum-to-resting metabolic rates (MMR/RMR), among all species with empirical estimates of both parameters.** Blue dots, species with empirical estimates of both parameters (Supplementary Table 1). Lines of constant $w_R$ (see equation (9)) are shown for a sustained metabolic rate that is equal to the resting rate (SMS = 1; $w_R$ = 1; blue line), the maximum metabolic rate (SMS = FAS; $w_R$ = 0; red line) or the mean apparent species value ($w_R$ = 0.4; green line) in which sustained the metabolic rate is approximately midway between minimal (resting) and maximal rates. Independent geochemical estimate of SMS based on carbon isotopes in the otoliths of Atlantic cod[28] are shown as a triangle.
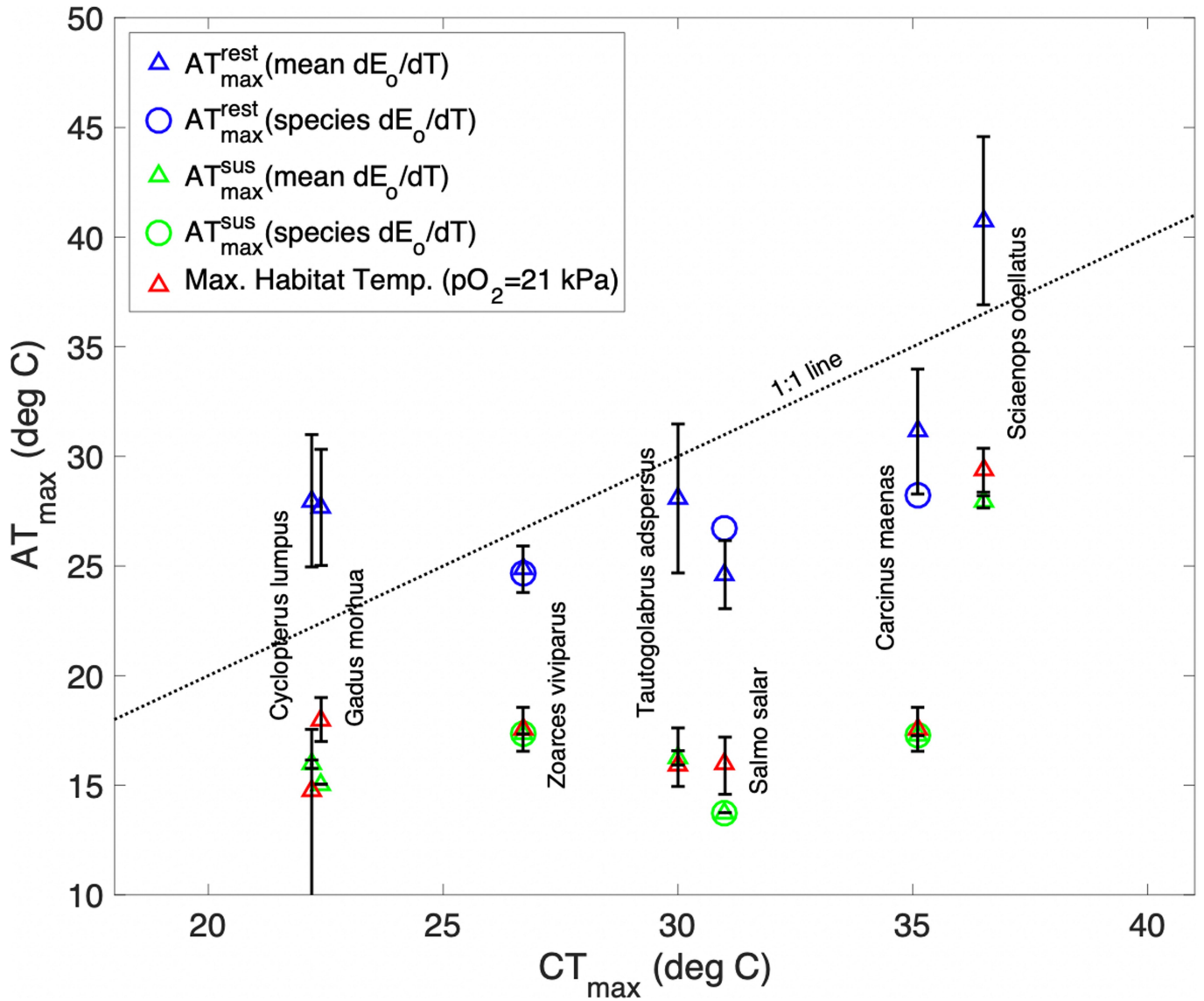
**Extended Data Fig. 10 | Relationship across species between thermal tolerance of species measured in laboratory studies and predicted from the Metabolic Index.** Critical thermal maxima ($CT_{max}$), reported in previous studies, were measured at the onset of loss of physiological function in a resting state. The $AT_{max}$ are predicted from the Metabolic Index, as the temperature at which the $O_2$ threshold for metabolic rate in either resting state ($P_{crit}$) or under sustained activity levels ($P_{crit} \times \Phi_{crit}$), reaches the mean atmospheric $O_2$ pressure, $P_{atm}$ (see Methods, equation (10)). The extrapolation of $P_{crit}$ curves to the atmospheric pressure is based on $n = 3$ independent estimates of the linear increase in $E_o$ with temperature (see Methods). Points for each species are the mean, and error bars show the range among the resulting $n = 3$ estimates of $AT_{max}$. Data are shown for all species in Fig. 5, for which all parameters are available ($n = 7$). For four out of seven species, the $AT_{max}$ is reached before the $CT_{max}$, even in a resting state. For all seven species, the active $AT_{max}$ is reached at a lower temperature than the $CT_{max}$, and is comparable to the maximum temperature that the species inhabits at atmospheric pressure.

**Extended Data Table 1 | Summary statistical tests of the relationships between metabolic and hypoxia traits and between distributions of $\Phi_{crit}$ and SMS**

| Relationship | Statistical Test | Coefficients (+95% C.I.) | Correl. ($r^2$) | P value | #obs (n) | Figures |
|---|---|---|---|---|---|---|
| $\alpha_S = a\,\alpha_D + b$ | Linear regression 2-sided t-test | Slope (a): 17.0 (13.3, 20.7) Inter. (b): 32.0 (3.5, 60.5) | 0.65 | 5.1e-12 | 48 | Fig. 1F ED Fig. 2A |
| $E_o = a\,E_d + b$ | Linear regression 2-sided t-test | Slope (a): 0.59 (0.43-0.75) Inter. (b): -0.02 (-0.13, 0.09) | 0.55 | 1.5e-9 | 48 | Fig. 1G |
| $E_s = a\,E_d + b$ | Linear regression 2-sided t-test | Slope (a): 0.40 (0.24,0.56) Inter. (b): 0.02 (-0.09, 0.13) | 0.36 | 6.5e-6 | 48 | ED Fig. 2B |
| $\Phi_{crit} = a\,V_h + b$ | Linear regression 2-sided t-test | Slope (a): -0.19 (-0.29, -0.09) Inter. (b): 4.05 (3.5, 4.6) | 0.22 | 2.8e-4 | 56 | ED Fig. 2C |
| $\Phi_{crit} = a\,FAS + b$ (FAS=MMR/RMR) | Linear regression 2-sided t-test | Slope (a): 0.55 (0.37, 0.74) Inter. (b): 0.65 (-0.26, 1.55) | 0.78 | 3.2e-5 | 14 | ED Fig. 8 |
| $\Phi_{crit}$ vs SMS (terrestrial) | Kolmogorov-Smirnov (2-sample) | N/A | N/A | 0.79 | 58, 50 | Fig. 4A,C |
| $\Phi_{crit}$ vs SMS (marine) | Kolmogorov-Smirnov (2-sample) | N/A | N/A | 0.67 | 58, 76 | Fig. 4A,B |
| SMS (marine) vs SMS (terr.) | Kolmogorov-Smirnov (2-sample) | N/A | N/A | 0.47 | 76, 50 | Fig. 4B,C |

All correlations are determined by standard linear regression (computed using MATLAB's function regress.m) and indicate statistically significant relationships ($P < 0.05$) between traits. All comparisons among histograms were evaluated by a two-sample Kolmogorov–Smirnov tests and indicate that significant differences in the underlying frequency distributions cannot be detected ($P > 0.05$) with the data.

Corresponding author(s): Curtis Deutsch

Last updated by author(s): May 27, 2020

# Reporting Summary

Nature Research wishes to improve the reproducibility of the work that we publish. This form provides structure for consistency and transparency in reporting. For further information on Nature Research policies, see Authors & Referees and the Editorial Policy Checklist.

## Statistics

For all statistical analyses, confirm that the following items are present in the figure legend, table legend, main text, or Methods section.

| n/a | Confirmed | |
|---|---|---|
| ☐ | ☒ | The exact sample size ($n$) for each experimental group/condition, given as a discrete number and unit of measurement |
| ☒ | ☐ | A statement on whether measurements were taken from distinct samples or whether the same sample was measured repeatedly |
| ☐ | ☒ | The statistical test(s) used AND whether they are one- or two-sided *Only common tests should be described solely by name; describe more complex techniques in the Methods section.* |
| ☒ | ☐ | A description of all covariates tested |
| ☒ | ☐ | A description of any assumptions or corrections, such as tests of normality and adjustment for multiple comparisons |
| ☐ | ☒ | A full description of the statistical parameters including central tendency (e.g. means) or other basic estimates (e.g. regression coefficient) AND variation (e.g. standard deviation) or associated estimates of uncertainty (e.g. confidence intervals) |
| ☐ | ☒ | For null hypothesis testing, the test statistic (e.g. $F$, $t$, $r$) with confidence intervals, effect sizes, degrees of freedom and $P$ value noted *Give P values as exact values whenever suitable.* |
| ☒ | ☐ | For Bayesian analysis, information on the choice of priors and Markov chain Monte Carlo settings |
| ☒ | ☐ | For hierarchical and complex designs, identification of the appropriate level for tests and full reporting of outcomes |
| ☐ | ☒ | Estimates of effect sizes (e.g. Cohen's $d$, Pearson's $r$), indicating how they were calculated |

*Our web collection on statistics for biologists contains articles on many of the points above.*

## Software and code

Policy information about availability of computer code

| Data collection | No new data was collected for this study. Published data was analyzed using software described below |
|---|---|
| Data analysis | The manuscript specifies that data analysis was conducted using Matlab software, and a link is provided to the analysis code on Github. |

For manuscripts utilizing custom algorithms or software that are central to the research but not yet described in published literature, software must be made available to editors/reviewers. We strongly encourage code deposition in a community repository (e.g. GitHub). See the Nature Research guidelines for submitting code & software for further information.

## Data

Policy information about availability of data

All manuscripts must include a data availability statement. This statement should provide the following information, where applicable:

- Accession codes, unique identifiers, or web links for publicly available datasets
- A list of figures that have associated raw data
- A description of any restrictions on data availability

The data used in this study are all publicly available and provided as a Table in Extended Data file. The codes are available on Github.

# Field-specific reporting

Please select the one below that is the best fit for your research. If you are not sure, read the appropriate sections before making your selection.

☐ Life sciences   ☐ Behavioural & social sciences   ☒ Ecological, evolutionary & environmental sciences

For a reference copy of the document with all sections, see nature.com/documents/nr-reporting-summary-flat.pdf

# Ecological, evolutionary & environmental sciences study design

All studies must disclose on these points even when the disclosure is negative.

| | |
|---|---|
| Study description | We analyzed experimental data compiled from numerous previously published studies. Our analysis procedure is detailed in Methods, and the experimental details of each study can be found in the original publications. |
| Research sample | Our study included data from all prior studies we could find that reported critical oxygen pressure at multiple temperatures for any marine aerobic species. |
| Sampling strategy | N/A |
| Data collection | Numerical data were taken from tables, text, and/or digitized graphs in the original publications. |
| Timing and spatial scale | N/A |
| Data exclusions | We excluded species whose environmental conditions in native habitats could not be characterized with available spatial datasets. |
| Reproducibility | N/A |
| Randomization | N/A |
| Blinding | N/A |

Did the study involve field work? ☐ Yes ☒ No

# Reporting for specific materials, systems and methods

We require information from authors about some types of materials, experimental systems and methods used in many studies. Here, indicate whether each material, system or method listed is relevant to your study. If you are not sure if a list item applies to your research, read the appropriate section before selecting a response.

## Materials & experimental systems

| n/a | Involved in the study |
|---|---|
| ☒ | ☐ Antibodies |
| ☒ | ☐ Eukaryotic cell lines |
| ☒ | ☐ Palaeontology |
| ☒ | ☐ Animals and other organisms |
| ☒ | ☐ Human research participants |
| ☒ | ☐ Clinical data |

## Methods

| n/a | Involved in the study |
|---|---|
| ☒ | ☐ ChIP-seq |
| ☒ | ☐ Flow cytometry |
| ☒ | ☐ MRI-based neuroimaging |